NACA RM L57J23a

NACA

# RESEARCH MEMORANDUM

## AN INVESTIGATION OF THE DRAG CHARACTERISTICS OF SPEED BRAKES FOR MACH NUMBERS FROM 0.20 TO 1.30

By Allen R. Vick

Langley Aeronautical Laboratory
Langley Field, Va.

NATIONAL ADVISORY COMMITTEE
FOR AERONAUTICS

WASHINGTON
January 13, 1958
Declassified March 18, 1960

NATIONAL ADVISORY COMMITTEE FOR AERONAUTICS

RESEARCH MEMORANDUM

# AN INVESTIGATION OF THE DRAG CHARACTERISTICS OF SPEED BRAKES FOR MACH NUMBERS FROM 0.20 TO 1.30

By Allen R. Vick

## SUMMARY

Drag characteristics of a series of aerodynamic speed brakes have been investigated over a range of stream Mach numbers from 0.20 to 1.30. The effects of brake deflection angle and aspect ratio, of brake chord relative to boundary-layer thickness, and of Mach number are shown in the form of design charts. It is shown that for all aspect ratios the drag coefficient is strongly dependent on the ratios of brake chord and brake projected height to the boundary-layer thickness. The brake drag coefficient was more dependent on boundary-layer thickness at small deflection angles than at large deflection angles. The drag coefficient obtained in the presence of a small amount of boundary layer was generally greater than that obtained with a comparable flat plate in a uniform stream. Minimum drag coefficient almost always occurs for brakes with aspect ratios of approximately 2. Additional tests with side plates added to the brakes show that for most conditions higher drag coefficients may be obtained by the use of side plates.

## INTRODUCTION

Aerodynamic braking of aircraft for many years was used only as a means of limiting velocity in a dive or to reduce the landing approach speed. As aircraft speeds have increased, changing fighter tactics have increased the demand for rapid deceleration, and new applications in the form of control devices for missiles and aircraft have appeared. Although the problem of aerodynamic braking at high speeds is not entirely new, only a limited amount of data is available and no systematic study has appeared. In reference 1, a summary of available low-speed data is presented for a wide variety of brakes, but only a small percentage of these data is suitable for fuselage applications because the brakes used were

generally of high aspect ratio (equal to or greater than 2). A study of high-drag devices applicable to missile recovery is presented in reference 2 for Mach numbers up to 5.0; however, very little test data are presented. Most of the data available from tests of fuselage-type brakes are restricted to specific developmental programs. Attempts to correlate existing data have been unsuccessful due to inadequate information about individual tests.

The present investigation was initiated to provide a systematic study of the effects of certain geometric parameters on the transonic drag characteristics of deflected brakes. Test data are presented over a Mach number range from 0.20 to 1.30 with the corresponding Reynolds number per inch varying from $0.1 \times 10^6$ to $0.6 \times 10^6$. Brakes of aspect ratio 0.25, 0.50, 1.00, 2.00, and 4.00 were tested at several deflection angles varying from $15^\circ$ to $90^\circ$. Other variables investigated included the ratios of brake height and brake chord to wall boundary-layer thickness. These data have been cross-plotted and are presented in a series of design charts.

## SYMBOLS

| | |
|---|---|
| $A$ | aspect ratio, $W/R$ |
| $C_D$ | brake drag coefficient, $D/qS$ |
| $D$ | total drag, lb |
| $H$ | projected height of brake, in. |
| $M$ | free-stream Mach number |
| $q$ | free-stream dynamic pressure, $\rho U_o^2/2$, lb/sq ft |
| $R$ | radius (chord) of brake, in. |
| $S$ | brake projected area, $WR \sin \alpha$, sq in. |
| $U$ | velocity within boundary layer, ft/sec |
| $U_o$ | free-stream velocity, ft/sec |
| $W$ | width of brake (span), in. |
| $\alpha$ | brake deflection angle, deg |

$\delta$ boundary-layer thickness at $\frac{U}{U_o} = 0.95$, in.

$\rho$ density, slugs/cu ft

## APPARATUS AND METHOD

The transonic tunnel used in this investigation was a continuous operation, nonreturn system with a slotted test section $4\frac{1}{2}$ by $6\frac{1}{4}$ inches in cross section and 17 inches in length. (See fig. 1.) The test section was slotted in one wall only. A chamber beneath the slotted bottom floor was connected to a vacuum pump, and Mach numbers above 0.95 were obtained by regulating the chamber pressure with the tunnel total pressure remaining constant. The top wall of the tunnel was solid with a circular cutout into which a force dynamometer was mounted. All models therefore projected downward from the top of the tunnel. Surveys of the tunnel flow along the solid wall (reflection plane) have shown negligible pressure gradients in the region in which the models were mounted.

Models were of identical basic construction; they consisted of 1/16-inch-thick flat plates attached to a 1/8-inch-diameter rod which was inserted in the force-dynamometer support sleeve. The models tested varied in aspect ratios from 0.25 to 4.00 with deflection angles varying from $15^{\circ}$ to $90^{\circ}$. The brake deflection angles, the radii, the heights, and the corresponding aspect ratios of the models tested in this investigation are given in table I. Also shown in table I is a generalized sketch defining the various symbols used to identify the models. A few models of solid construction (closed sides) were tested to determine the effects of side plates. A clearance gap of 0.004 inch was maintained between the models and tunnel wall. All models were alined perpendicular to the flow.

The force dynamometer was of the floating-body type and is shown in the photograph in figure 2. Basically, it consists of a floating body supported by two flat cantilever springs. All streamwise loads applied to the models are transmitted directly to an unbonded strain-gage element whose output was fed into a continuously recording potentiometer. The base of the force dynamometer was inserted in a circular cutout in the top wall of the tunnel so as to be flush with the surface. The floating part of the balance was insulated electrically from the tunnel, and a light was installed to warn of any contact between the balance and surrounding structure. Maximum movement of the floating body for full strain-gage deflection was 0.0015 inch. The unbonded strain gage was mounted on a water-cooled pad in order to maintain the gage at a constant temperature. Continuously recording potentiometers were also used to record

stream pressures required to compute Mach number. Base pressure measurements were obtained by placing a single total-pressure probe approximately 1/32 inch downstream of, and in the approximate geometric center of, the speed brake. Pressure transducers were located close to the measuring point to eliminate possible pressure lags. The speed, starting at a Mach number of 0, was increased slowly and data were recorded continuously. A time interval of approximately 3 minutes was required to obtain data over a Mach number range from 0.20 to 1.30. Check runs made with decreasing speed showed only minor differences in the results. Boundary-layer measurements were obtained from a vertical survey of the total pressure distribution as obtained from a series of total-pressure tubes located in the region where the models were mounted.

In order to obtain a reference from which to evaluate boundary-layer effects, tests of a series of sting-mounted flat plates were conducted in a larger transonic tunnel (10- by 10-inch test section). Two walls of this tunnel were slotted and the models were sting supported on the tunnel axis. Operation of this larger tunnel was identical to that of the smaller facility.

## RESULTS AND DISCUSSION

Since most of the fuselage-type speed brakes in use on existing planes are located well back on the fuselage, these brakes generally operate in a boundary layer of considerable thickness. The variation of wall boundary-layer thickness with Mach number for this investigation is shown in figure 3. This boundary-layer thickness is defined as the height at the point where the ratio of the velocity within the boundary layer to the free-stream velocity is 0.95. As shown in the figure, there is a continuous decrease in boundary-layer thickness with increasing Mach number. The boundary-layer thickness is relatively constant up to $M = 0.40$; as the Mach number increases from 0.40 to 1.30, the boundary-layer thickness decreases but appears to be leveling out at the high Mach numbers. The boundary-layer profiles indicated turbulent flow at all speeds.

### Data Presentation

The test data are presented as drag coefficient plotted against stream Mach number for constant brake angles of 15°, 30°, 45°, 60°, and 90° and aspect ratios of 0.25, 0.50, 1.00, 2.00, and 4.00. (See figs. 4 to 8.) Drag coefficient is defined in terms of the brake projected area. Test points in the individual figures indicate different radii of the models tested. The individual data points appearing in

the figures were computed at specific intervals as obtained from a continuous plot of drag against Mach number. Slight scatter in the data points, particularly at the lower Mach numbers, is within the accuracy of reading from the continuous data plots.

The variation of drag coefficient with Mach number (figs. 4 to 8) shows that below the drag rise the value of $C_D$ increases slowly for the lower deflection angles and aspect ratios and at a greater rate as these parameters increase. With increasing aspect ratio and/or brake deflection, the magnitude of the drag rise also tends to increase, and the Mach number at which it occurs shifts downward and becomes less clearly defined. At stream Mach numbers slightly less than unity, local sonic velocities are obtained on the edges of the various brakes and the resulting expansion that is reflected from the opposite wall decreases the base pressure and thus gives values of $C_D$ that are too high. Over the general Mach number range from 1.00 to 1.20, the bow shock that is reflected from the tunnel wall increases the base pressure and results in values of $C_D$ which are too low. Both the expansion- and shock-reflection interference effects have been faired out as shown by the dashed sections of the curves. These dashed lines are considered to be more representative of free-air performance than a line through the data points. As Mach number increases, the reflected shock moves farther downstream and its influence disappears. The magnitude of the interference is determined largely by the brake projection normal to the stream; thus, increasing the brake angle extends the interference effect over a wider Mach number range. Increasing the radius also increases the interference speed range. As the brake radius increases, the drag coefficient generally increases. This increase is to be expected since a greater portion of the brake extending through the boundary layer is subjected to the higher stream velocity; the fact that this does not always occur (figs. 5(b), 5(c), and 6(b)) will be discussed later in connection with the design charts. All the drag curves (figs. 4 to 8) are similar in shape with the exception of the curves for a radius of 0.32 inch and aspect ratio of 0.50 in figures 6(b) and 8(a) where the irregularities are attributed to balance difficulties. These curves were faired out in preparing the design charts.

The drag coefficients of the sting-mounted models ($\alpha = 90^{\circ}$) are shown in figure 9 as a function of stream Mach number. Aspect ratio within the range of these tests (0.50 to 2.00) has no effect on the drag coefficient; the maximum variation, ±5 percent at low Mach numbers, is obtained in repeat tests with a single model rotated $90^{\circ}$. Agreement of the sting-mounted flat-plate data for similar models of different size suggests that the sting effect was small; however, no effort has been made to evaluate its magnitude. The variation of $C_D$ with Mach number for an inclined $85^{\circ}$ brake mounted approximately 1 brake radius away from the fuselage (ref. 1) is plotted in figure 9 and shows very

good agreement with the data from the current tests with the 90° brake. These coefficients are slightly lower than would have been expected from comparisons with other published reports; however, available data are generally limited to that obtained at very low Mach numbers ($M < 0.1$) and correspondingly low Reynolds numbers.

In order to facilitate evaluation of boundary-layer effects, the drag characteristics of two identical 90° brakes, one sting-mounted and the other wall-mounted, are superimposed in figure 10. These curves show that a wall-mounted model in the presence of a boundary layer has a higher total drag coefficient than a sting-mounted model at $M > 0.3$, and that the increment in $C_D$ increases throughout the Mach number range.

The higher drag coefficient for the wall-mounted model at Mach numbers less than 1.0 is a result of the higher base drag as shown in the lower part of figure 10. Through the subsonic speed range, the base drag coefficient is on the order of 40 percent greater than for the sting-mounted plate. Since this difference is substantially greater than that observed between the total-drag curves, it is evident that the forebody drag of the wall-mounted model must be reduced somewhat because of the presence of the boundary layer. At Mach numbers greater than 1.0, the presence of the boundary layer has little influence on the base drag coefficient as shown by the close proximity of the curves for the two models. The fact that the total-drag coefficient of the wall-mounted model still remains higher than that of the sting-mounted model, even though both have approximately the same base drag, indicates an abrupt decrease in the forebody drag of the sting-mounted model to a value less than that for the wall-mounted model. This is a complete reversal of the subsonic characteristics. Curves of both forebody and base pressure drag fair in favorably with the higher Mach number data of reference 2.

Schlieren photographs of two of the sting-mounted flat plates are presented in figure 11. At low speeds, the wake boundary has a slightly curved shape and extends a considerable distance on either side of the center line. As Mach number increases, no appreciable change in the wake profile is apparent. At $M = 1.01$ and 1.09 (fig. 11(a)), the fact that the bow shock waves appear fuzzy suggests that the flow was unsteady and the accompanying wake profiles are therefore not representative of steady-state flow conditions. At speeds just above $M = 1.00$ (fig. 11(b)), steady flow is indicated by the clearness of the bow wave; the wake boundary becomes almost parallel with the stream direction and appears to converge at the higher speeds. As a result of these changes, an abrupt increase occurs in the base pressure as Mach number increases from 0.95 to 1.05. (See fig. 10.) The increase in base drag resulting from these flow changes is nearly twice the increment obtained for the total drag at the same Mach number range.

## Design Charts

From the data of figures 4 to 8, a series of design charts have been drawn for Mach numbers of 0.20, 0.50, 0.90, and 1.30, and for constant values of aspect ratio varying from 0.50 to 4.00. These design charts were obtained by cross-plotting the results from the data figures to establish trends and define families of curves. Although individual points may show some scatter about these curves, the deviations are minor in most cases. These charts, presented in figure 12, show the brake drag coefficient as a function of the projected height of the brake relative to the boundary-layer thickness. The projected height is dependent upon both the brake chord and deflection angle, the effects of which have been separated in the design charts by presenting two sets of curves in each figure - one set showing $C_D$ plotted against $H/\delta$ for fixed values of $R/\delta$ and a second set along which $\alpha$ was constant. The boundary-layer thickness $\delta$ used to nondimensionalize the data varied with Mach number as previously shown. Thus, $\delta$ is a constant for each given Mach number in the design charts of figure 12 with the value of $\delta$ being obtained at the corresponding Mach number in figure 3.

A line of constant $R/\delta$ corresponds to a brake of given dimensions being deflected at different angles to the direction of flow with corresponding increases in brake height and $H/\delta$. For brakes of short chord, or small values of $R/\delta$, the value of $C_D$ increases rapidly as $H/\delta$ is increased by increasing the deflection angle. The rate of change of $C_D$ with $H/\delta$ is substantially reduced by increasing the brake chord. No evidence of any irregularity in the drag appears; thus, no abrupt changes in deceleration would be expected as the brakes were either opened or closed.

Along lines of a constant brake deflection angle, increases in brake height result from increases in the radius of the brake. Along these curves and at the highest deflection angles, the drag coefficient increased with increasing brake height to a maximum, which at aspect ratios of 0.50 and 1.00 occurred at values of $R/\delta$ on the order of 5 or 6 for subsonic Mach numbers. (See fig. 12.) For lower deflection angles, higher values of $R/\delta$ are required to reach a maximum drag coefficient because of the increased brake area immersed in the boundary layer. There thus exists an optimum ratio of brake chord to boundary-layer thickness ($R/\delta$) which will yield the highest drag coefficient. Further extensions of the brake chord led to losses in $C_D$ as previously observed in data figures 5(b), 5(c), and 6(b). It has been shown in figure 10 that the maximum value of $C_D$ for a $90^\circ$ brake extending through the boundary layer was higher than the value for a similar sting-supported flat plate set at $90^\circ$ to the free stream. It is evident that the drag for the wall-mounted brake must reach that for the sting-supported flat plate at an infinite value of $H/\delta$.

At the higher aspect ratios (2.00 and 4.00), the point of maximum $C_D$ is shifted to greater brake heights, in many cases beyond the scope of these tests. It is thus shown that the location of the maximum drag coefficient is a function of both the brake deflection angle and the ratio of brake height to boundary-layer thickness - the greater the deflection angle the higher the ratio of $H/\delta$ required.

The effects of aspect ratio are best shown by comparisons of curves for constant deflection angle. As aspect ratio increases from 0.50 to 2.00, the level of $C_D$ decreases for a given value of $H/\delta$ and constant deflection angle, followed by a short range of little change in $C_D$. With further increases in aspect ratio beyond 2, the drag coefficient begins to increase again. This result is similar to that reported in reference 3 for sting-mounted flat plates of varying aspect ratio. It is of interest to note that this trend holds true regardless of boundary-layer thickness or Mach number. At low values of $H/\delta$ the range in which aspect ratio has no effect on $C_D$ is considerable, but this range becomes much smaller as $H/\delta$ increases. At subsonic speeds, doubling the aspect ratio at $H/\delta$ = Constant, and thus the brake projected area, does not in general double the drag as can be noted by the decrease in $C_D$ as aspect ratio is increased from 0.50 to 1.00; some exceptions are noted at the lower deflection angles. On the other hand, increasing aspect ratio from 2.00 to 4.00 reverses the trend, with the $A = 4.00$ brake producing more than double the drag of the $A = 2.00$ brake.

Comparisons of the data obtained in this investigation with data from complete model tests of fuselage-type dive brakes (refs. 1 and 4 to 6) show no areas of major disagreement. Values of $C_D$ obtained from these references are tabulated on the appropriate design charts to facilitate comparison. It should be pointed out that in all comparisons of data from other reports it was necessary to assume a boundary-layer thickness. Thus, although this did not permit specific comparisons, results were in general of the same order of magnitude.

## Side-Plate Effects

A series of solid models were tested in an effort to determine what effect the addition of side plates would produce on the drag coefficient of speed brakes. Side closure was simulated by using solid triangular-shaped models. The results of these tests for deflection angles of $15^{\circ}$, $30^{\circ}$, and $45^{\circ}$ are shown in figure 13 for an aspect ratio of 2.00 and for Mach numbers of 0.50, 0.90, and 1.30. Since complete drag curves for the solid models (side-plate simulation tests) are not presented, the data points are indicated in this figure. Also plotted for comparison purposes are the results obtained for the open-sided models previously

discussed. Closed-sided brakes appear to offer considerable increase in drag under certain conditions. At $M = 0.50$ and $H/\delta$ = Constant, the change in drag due to the side closure increases as the brake deflection angle is increased from $15^{\circ}$ to $45^{\circ}$; however, there must be a decrease in $\Delta C_D$ at some higher brake angle since the configurations are identical at $\alpha = 90^{\circ}$. At $M = 0.90$, improvement is very small at the lower angles and a loss in drag is incurred at certain values of $H/\delta$; however, at $M = 1.30$, an increase in $C_D$ exists for each deflection angle tested. The greatest increase in drag coefficient was obtained at low values of $H/\delta$.

The effects of aspect ratio on the variation of $C_D$ with $H/\delta$ for open- and closed-sided speed brakes at a constant Mach number of 0.50 are shown in figure 14. No data points are presented for aspect ratios of 0.25, 0.50, and 1.00 because these curves were obtained from cross plots of unpublished data. The decrease in $C_D$ with increasing aspect ratio previously noted for the open-sided brakes is still evident for the brakes with side-plate attachments. Brakes with low deflection angles have a drag coefficient strongly dependent on both aspect ratio and the ratio of brake height to boundary-layer thickness ($H/\delta$). Brakes with closed sides and at deflection angles of $45^{\circ}$ yield much higher drag coefficients for all test aspect ratios.

## CONCLUDING REMARKS

From the results of this investigation of the drag characteristics of a series of speed brakes for Mach numbers from 0.20 to 1.30, design charts have been prepared from which it is possible to determine the performance characteristics of a wide range of configurations suitable for aerodynamic braking of aircraft. The following results are noted:

1. The drag coefficient of a given configuration is strongly dependent upon brake height relative to the boundary-layer thickness, and for every brake angle there exists an optimum ratio of brake height to boundary-layer thickness which will yield the highest value of drag coefficient.

2. The drag coefficient is more dependent on the boundary-layer thickness at small brake deflection angles than at large deflection angles.

3. Under some conditions a brake operating in the presence of a boundary layer has a higher drag coefficient than a similar brake in a uniform stream.

4. Brakes with aspect ratios of approximately 2 generally have less drag than those with higher or lower aspect ratios.

5. In general, closing the sides of speed brakes produces higher drag coefficients.

Langley Aeronautical Laboratory,
National Advisory Committee for Aeronautics,
Langley Field, Va., October 3, 1957.

## REFERENCES

1. Stephenson, Jack D.: The Effects of Aerodynamic Brakes Upon the Speed Characteristics of Airplanes. NACA TN 1939, 1949.

2. Wiant, Harry W., and Fredette, Raymond O.: A Study of High Drag Configurations As First Stage Decelerators. WADC Tech. Note 56-320, Wright Air Dev. Center, U. S. Air Force, July 1956.

3. Fail, R., Owen, T. B., and Eyre, R. C. W.: Preliminary Low Speed Wind Tunnel Tests on Flat Plates and Air Brakes: Flow, Vibration and Balance Measurements. C.P. No. 251, British A.R.C., 1956.

4. Summers, James L., Treon, Stuart L., and Graham, Lawrence A.: Wind-Tunnel Investigation at Mach Numbers from 0.8 to 1.4 of Static Longitudinal and Lateral-Directional Characteristics of an Unswept-Wing Airplane Model. NACA RM A56E22, 1956.

5. Wright, John B.: High-Speed Wind-Tunnel Tests of a 1/16-Scale Model of the D-558 Research Airplane. D-558-1 Speed Reduction Brake and Symmetrical-Profile Wing Characteristics. NACA RM L8B06, 1948.

6. Mattson, Axel T., and Loving, Donald L.: Force, Static Longitudinal Stability, and Control Characteristics of a 1/16-Scale Model of the Bell XS-1 Transonic Research Airplane at High Mach Numbers. NACA RM L8A12, 1948.

TABLE I.- GEOMETRIC PARAMETERS OF DEFLECTED BRAKES

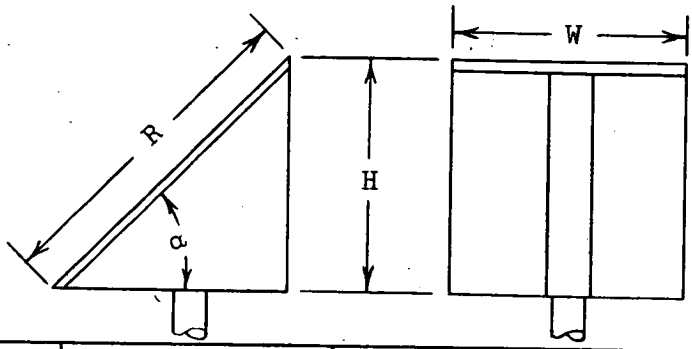


| R, in. | H, in. | Test aspect ratio, W/R |
|---|---|---|
| $\alpha = 15^{\circ}$ (see fig. 4) | | |
| 1.00 | 0.259 | 0.50, 1.00, and 2.00 |
| .75 | .194 | 0.50, 1.00, 2.00, and 4.00 |
| .50 | .129 | 1.00, 2.00, and 4.00 |
| $\alpha = 30^{\circ}$ (see fig. 5) | | |
| 1.00 | 0.500 | 0.25, 0.50, 1.00, and 2.00 |
| .75 | .375 | 0.50, 1.00, 2.00, and 4.00 |
| .50 | .250 | |
| $\alpha = 45^{\circ}$ (see fig. 6) | | |
| 1.00 | 0.707 | 0.25, 0.50, 1.00, and 2.00 |
| .75 | .530 | 0.50, 1.00, 2.00, and 4.00 |
| .64 | .453 | |
| .32 | .226 | |
| $\alpha = 60^{\circ}$ (see fig. 7) | | |
| 0.64 | 0.554 | 0.50, 1.00, and 2.00 |
| .50 | .433 | 0.50, 1.00, 2.00, and 4.00 |
| .32 | .277 | |
| $\alpha = 90^{\circ}$ (see fig. 8) | | |
| 0.64 | 0.640 | 0.50 and 1.00 |
| .50 | .500 | |
| .32 | .320 | |

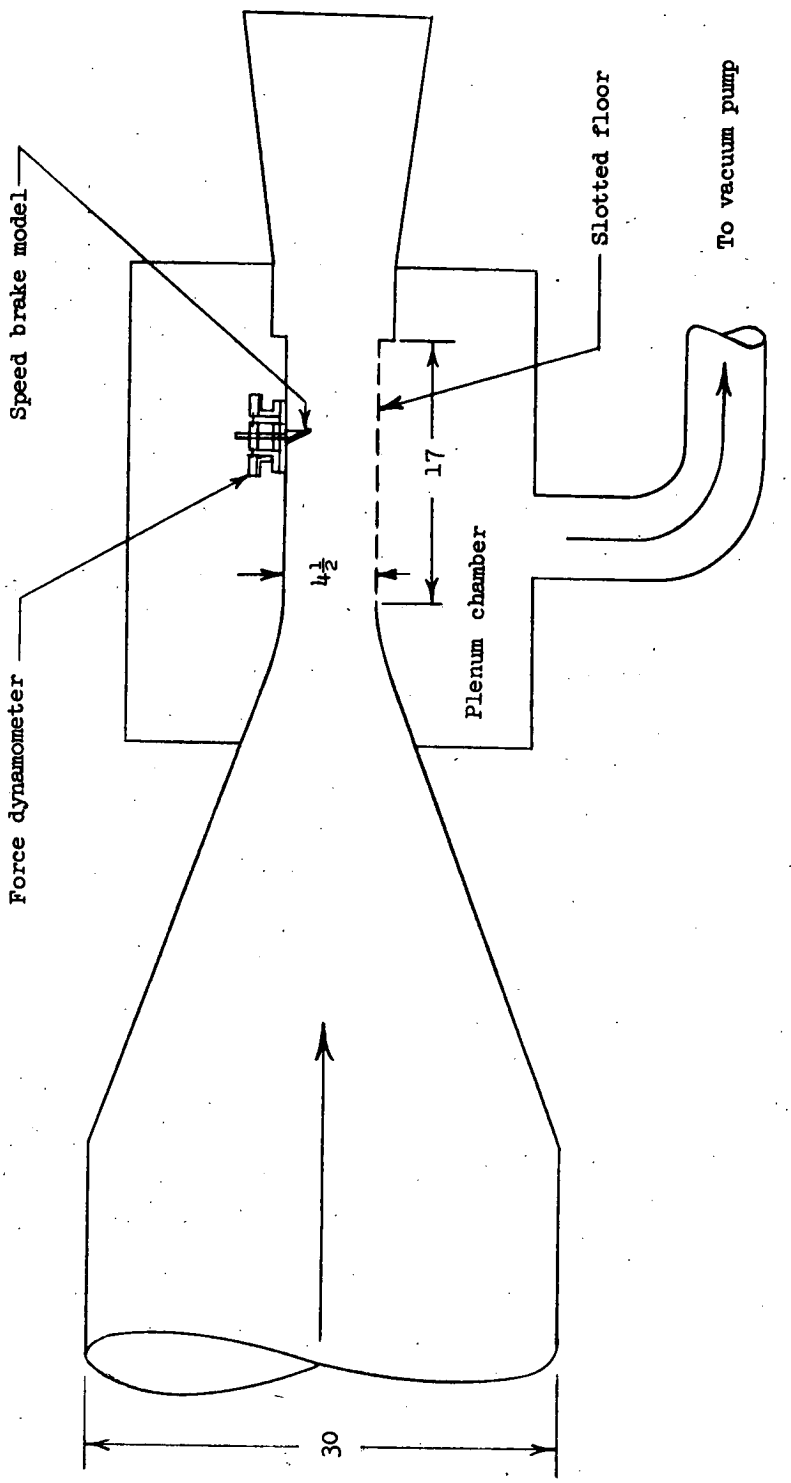


Figure 1.- General arrangement of tunnel with force dynamometer and speed brake installed. All dimensions are in inches.

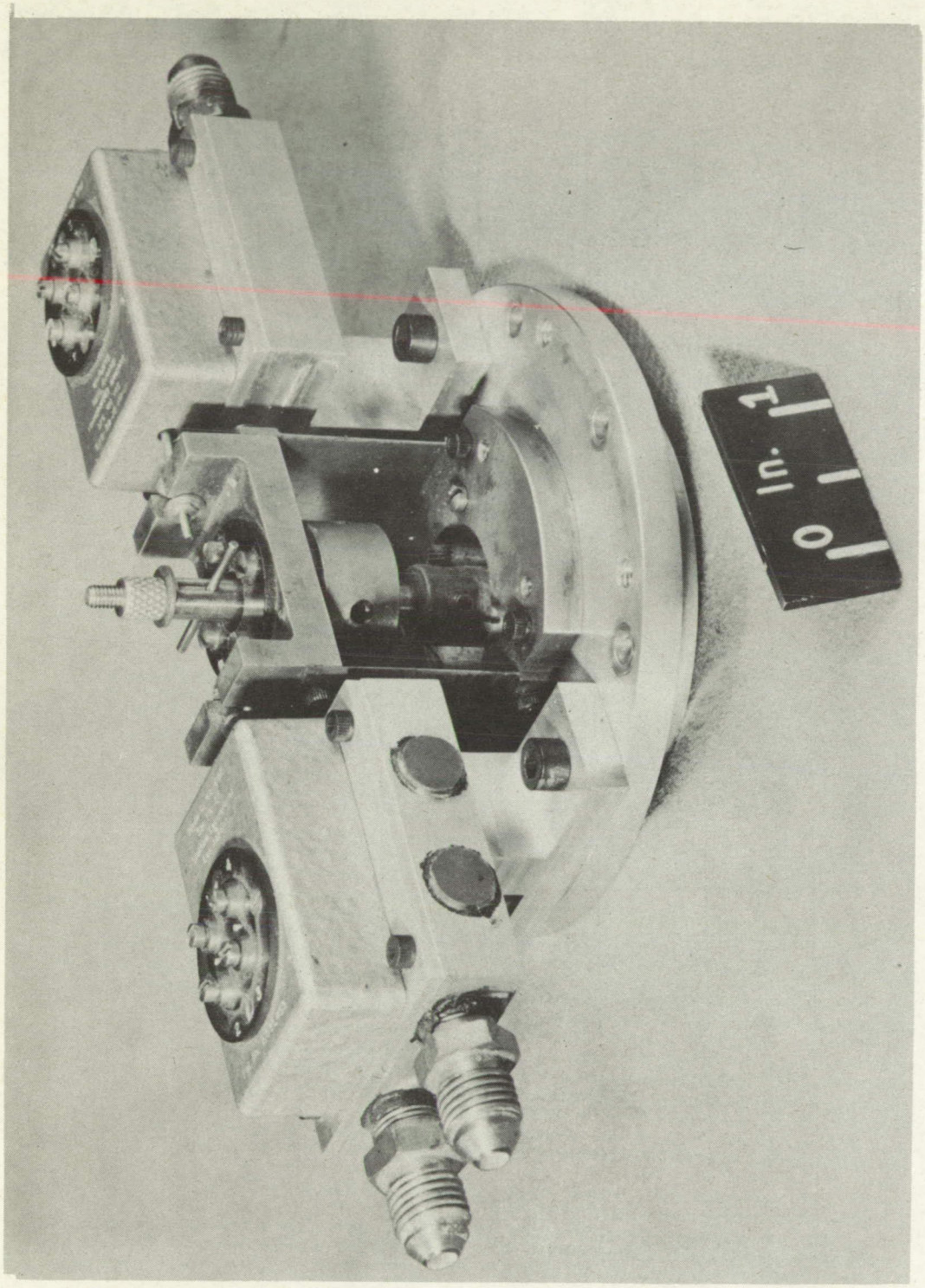


Figure 2.- Photograph of force dynamometer. L-57-1499

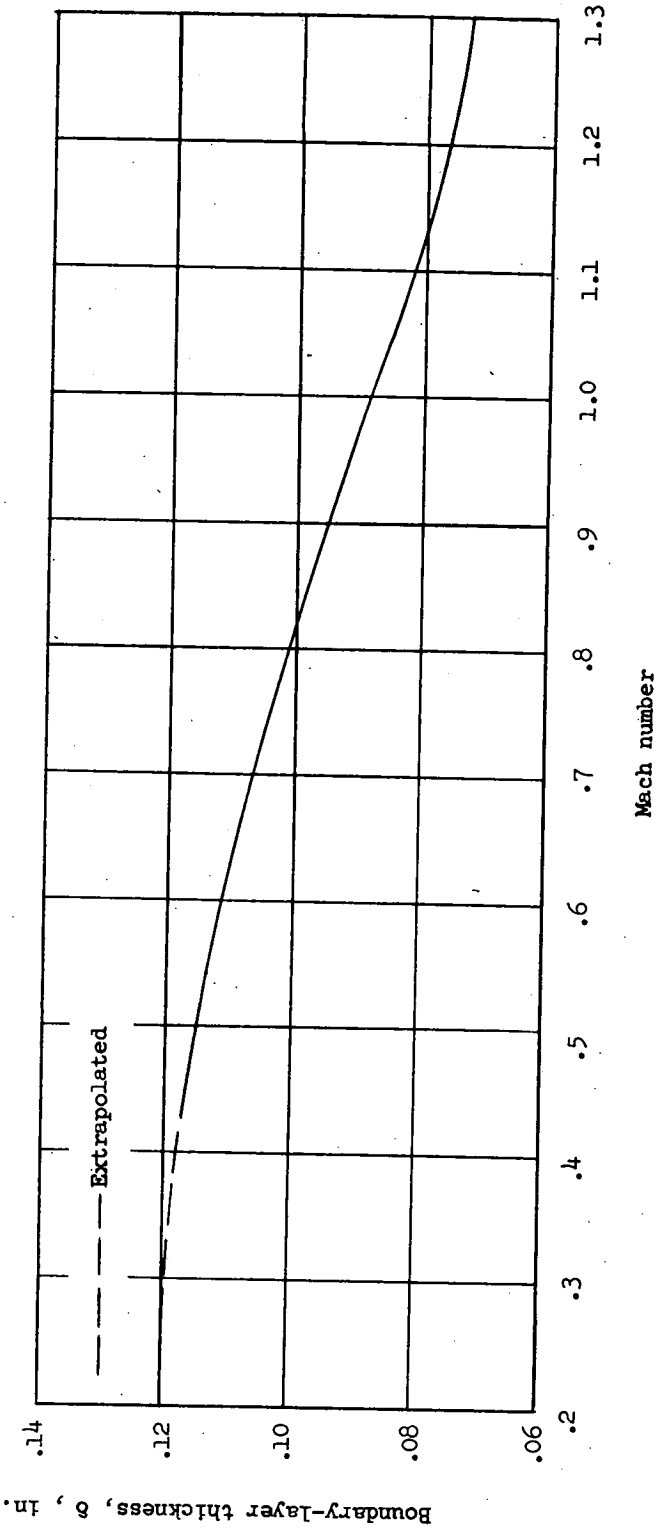


Figure 3.- Variation of boundary-layer thickness (at $U/U_o = 0.95$) with Mach number.

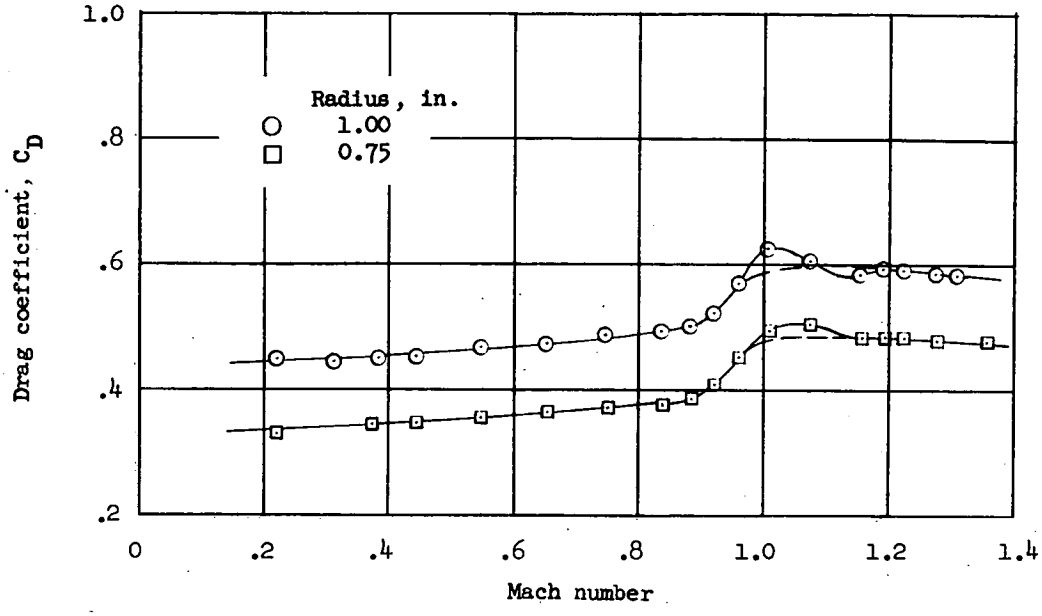


(a) Aspect ratio, 0.50.

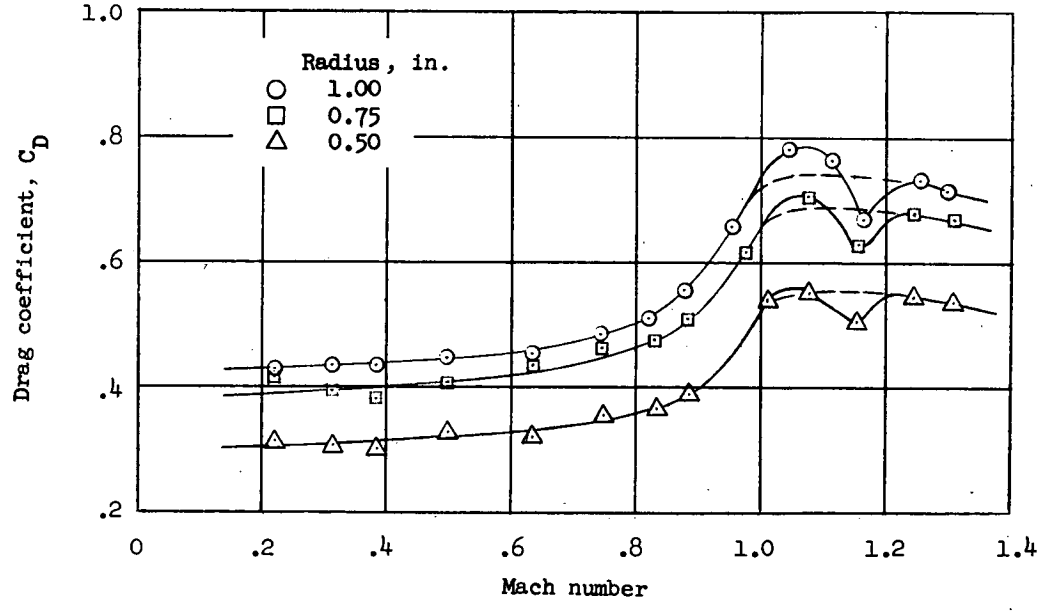


(b) Aspect ratio, 1.00.

Figure 4.- Variation of brake drag coefficient with Mach number for a deflection angle of 15°.

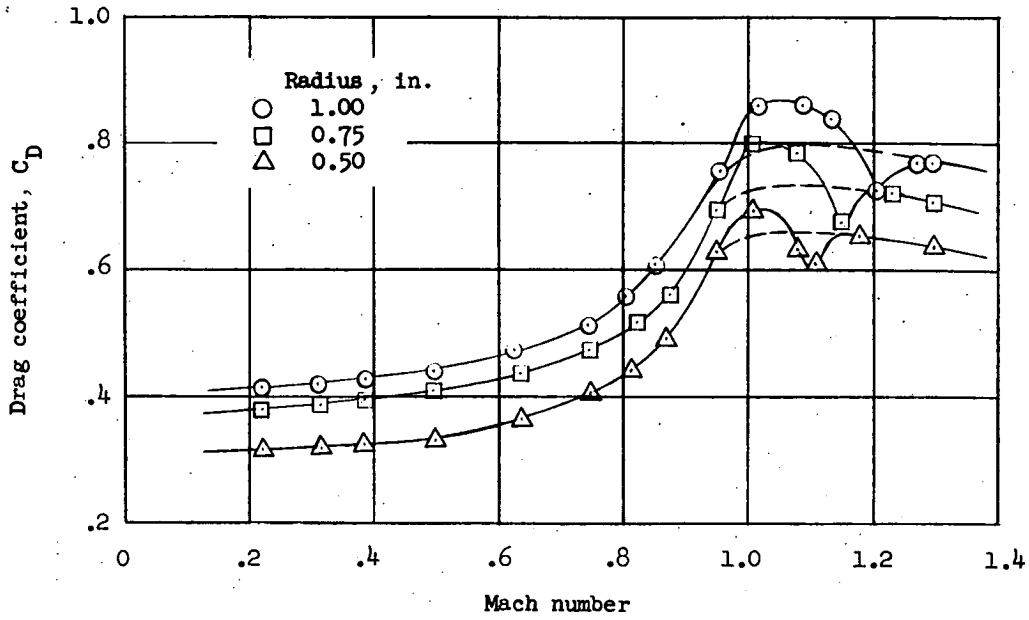


(c) Aspect ratio, 2.00.

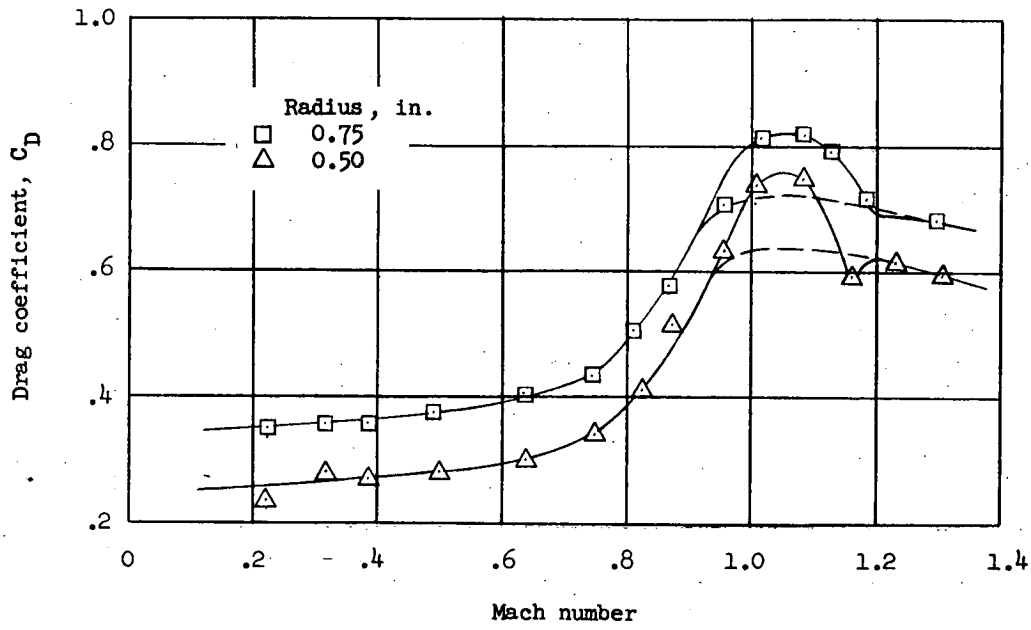


(d) Aspect ratio, 4.00.

Figure 4.- Concluded.

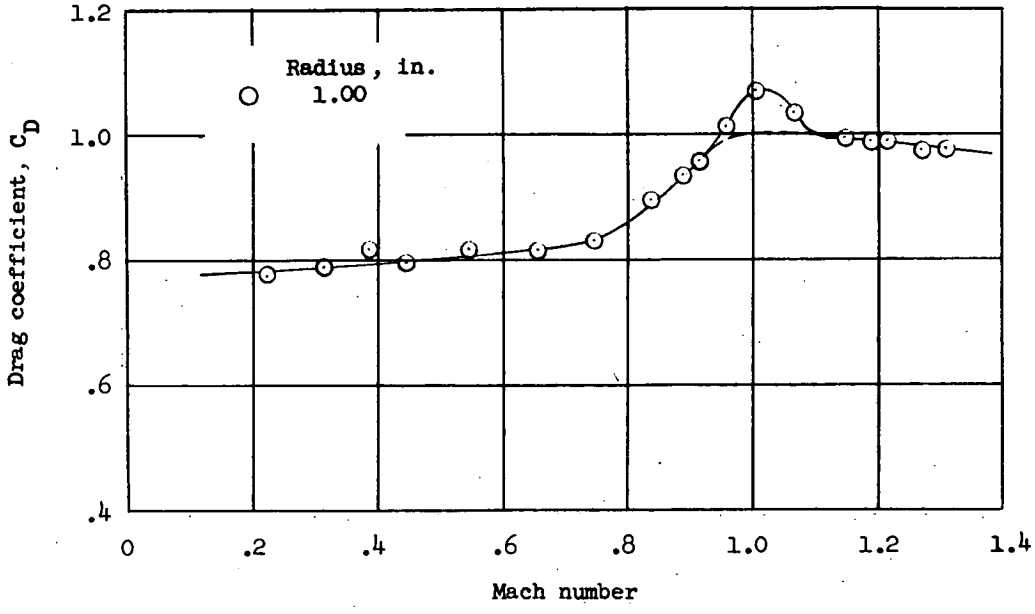


(a) Aspect ratio, 0.25.

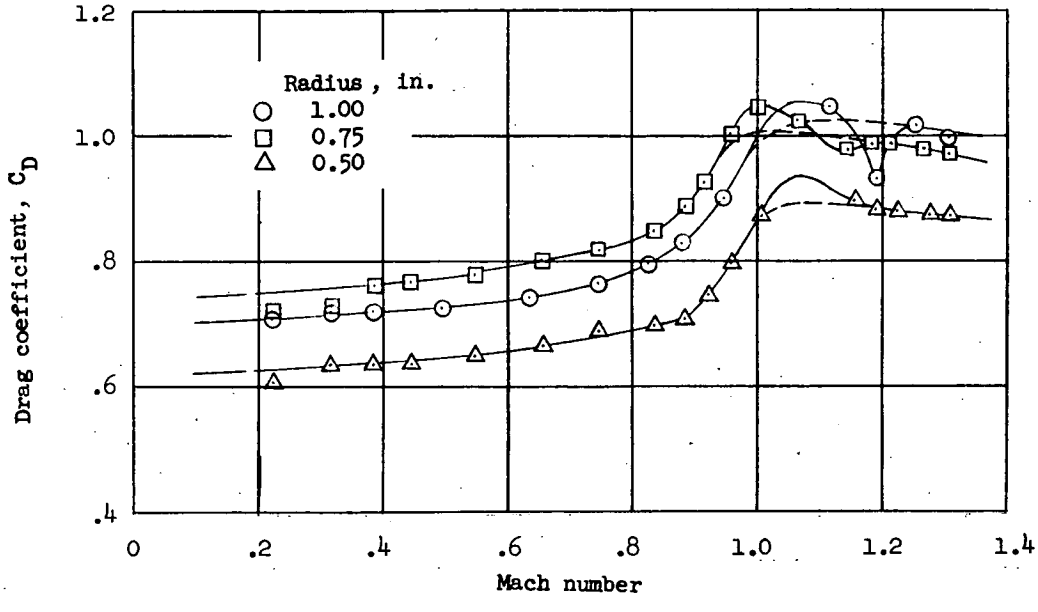


(b) Aspect ratio, 0.50.

Figure 5.- Variation of brake drag coefficient with Mach number for a deflection angle of 30°.

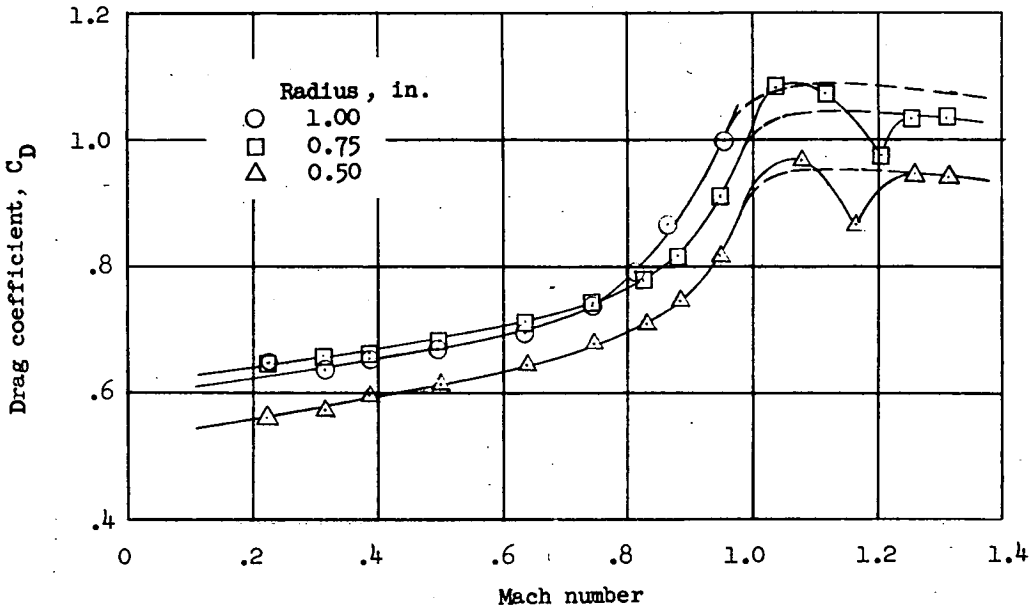


(c) Aspect ratio, 1.00.

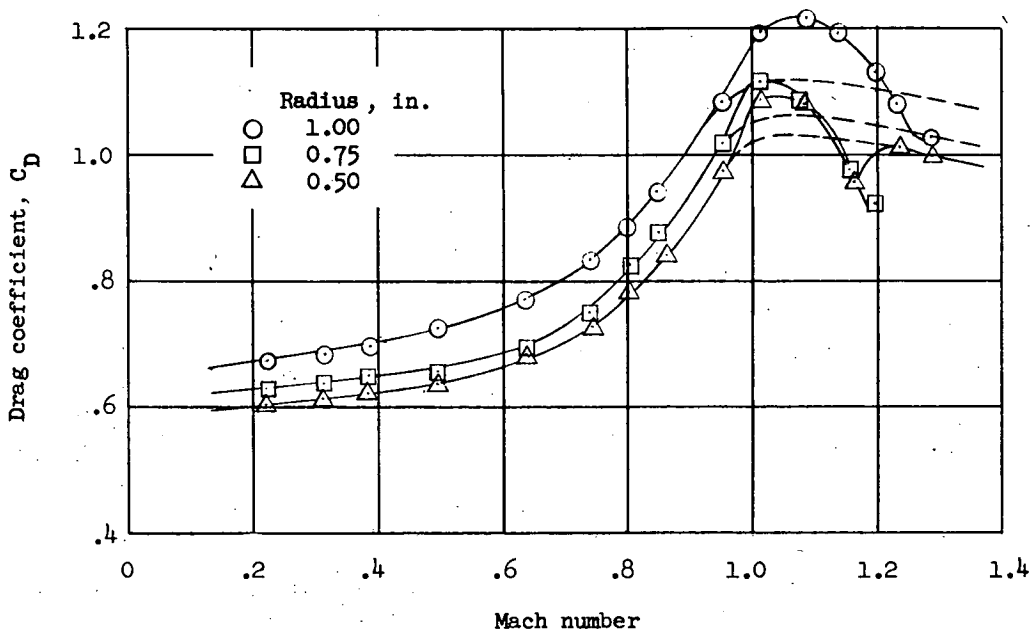


(d) Aspect ratio, 2.00.

Figure 5.- Continued.

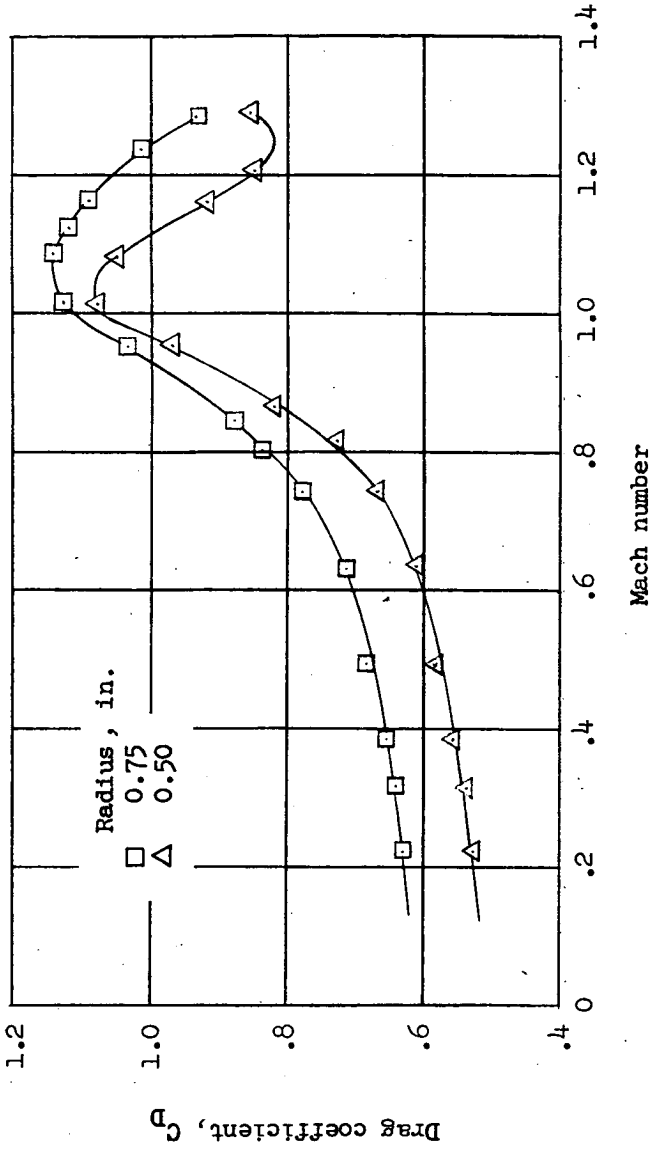


(e) Aspect ratio, 4.00.

Figure 5.- Concluded.

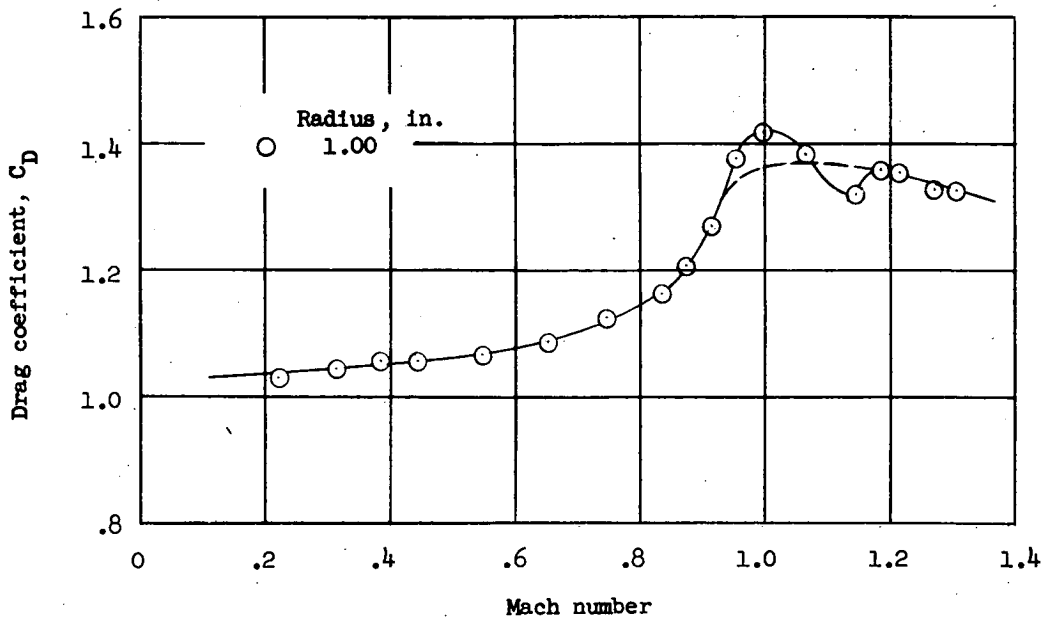


(a) Aspect ratio, 0.25.

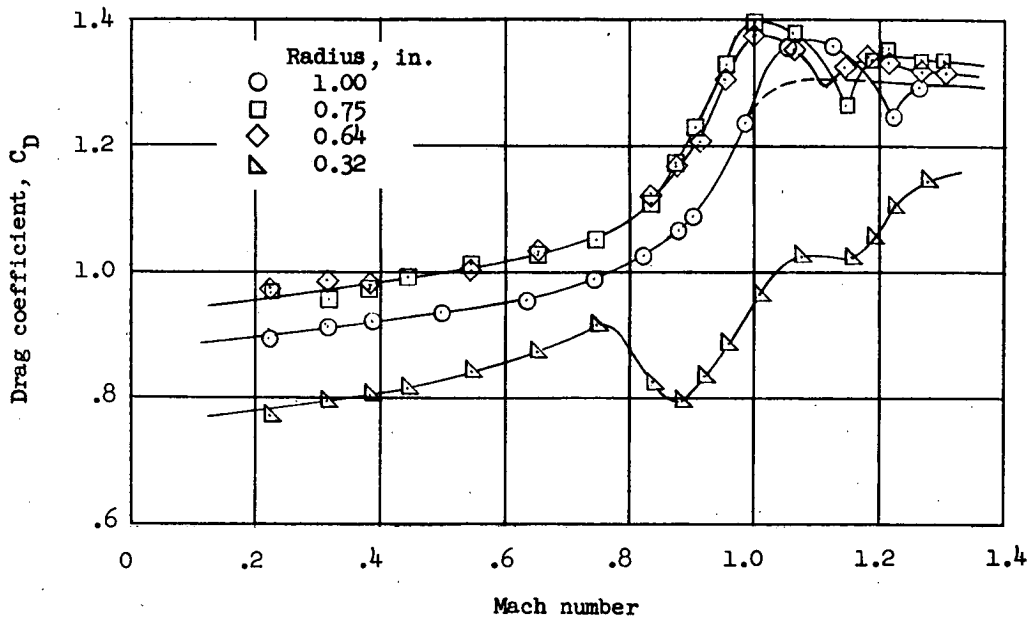


(b) Aspect ratio, 0.50.

Figure 6.- Variation of brake drag coefficient with Mach number for a deflection angle of 45°.

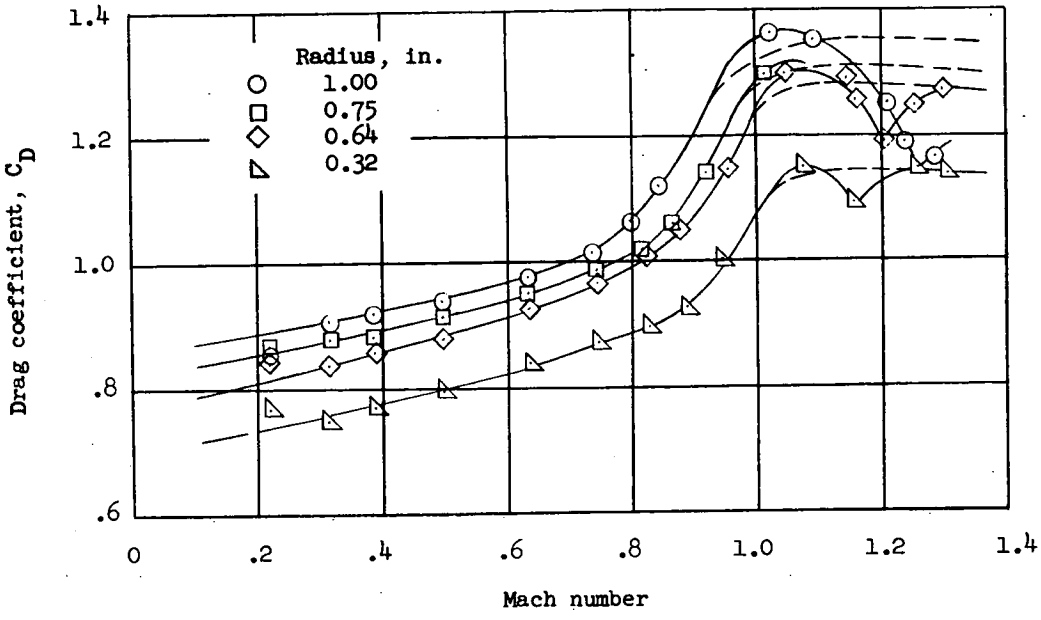


(c) Aspect ratio, 1.00.

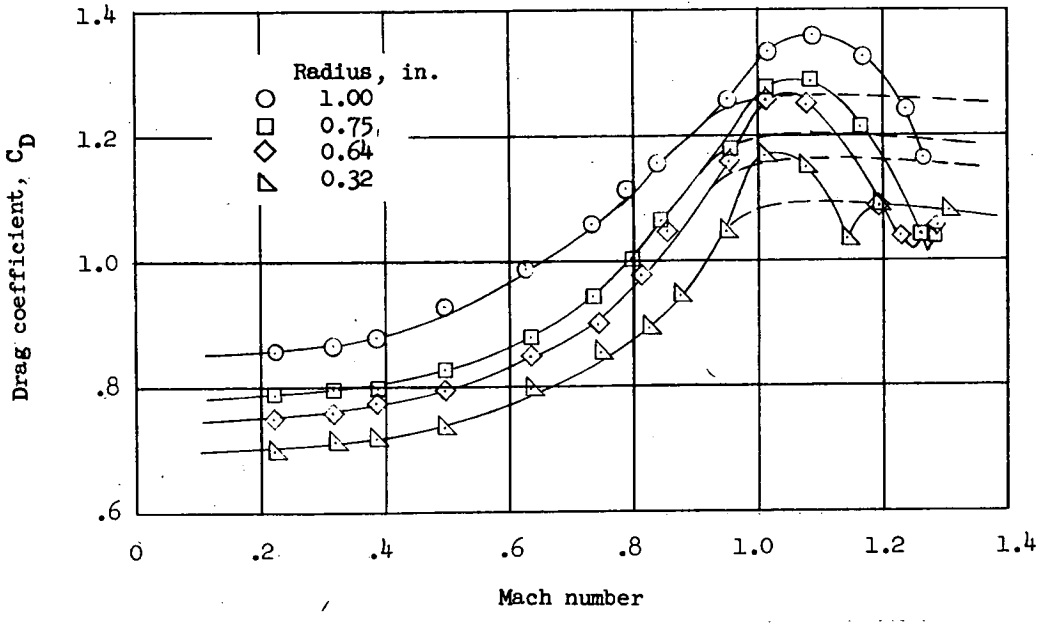


(d) Aspect ratio, 2.00.

Figure 6.- Continued.

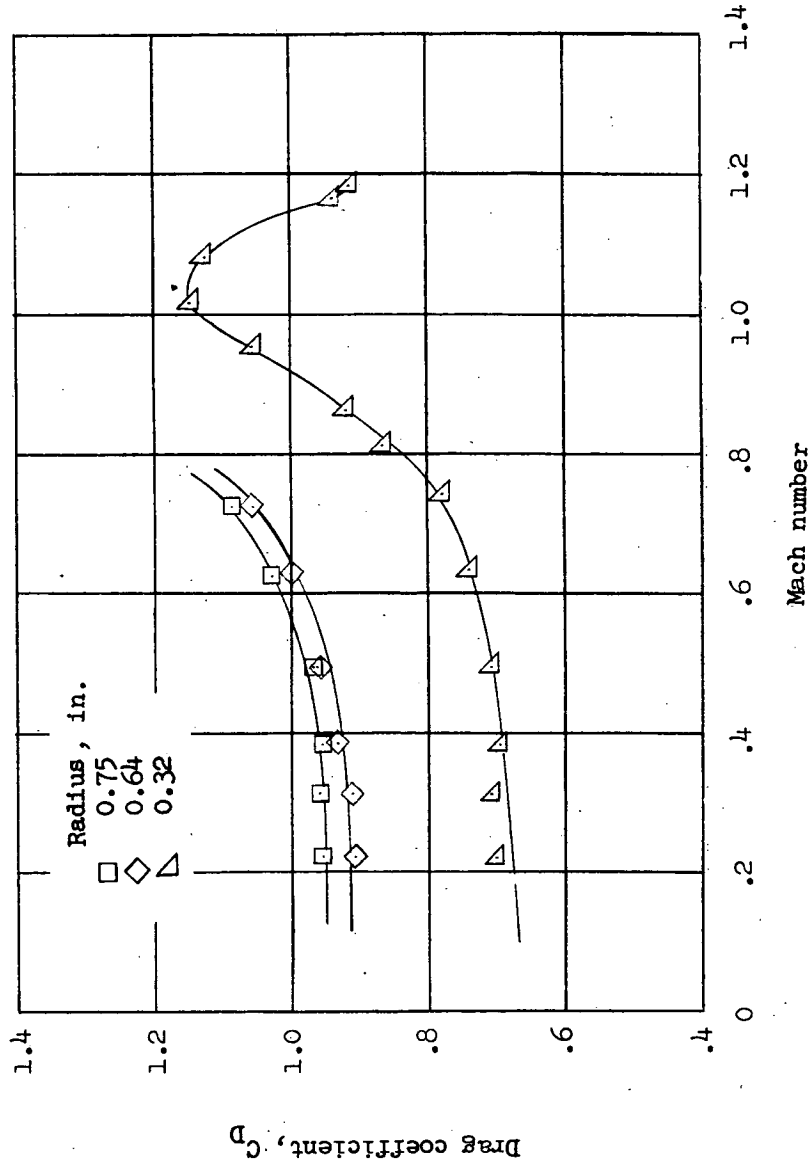


(e) Aspect ratio, 4.00.

Figure 6.- Concluded.

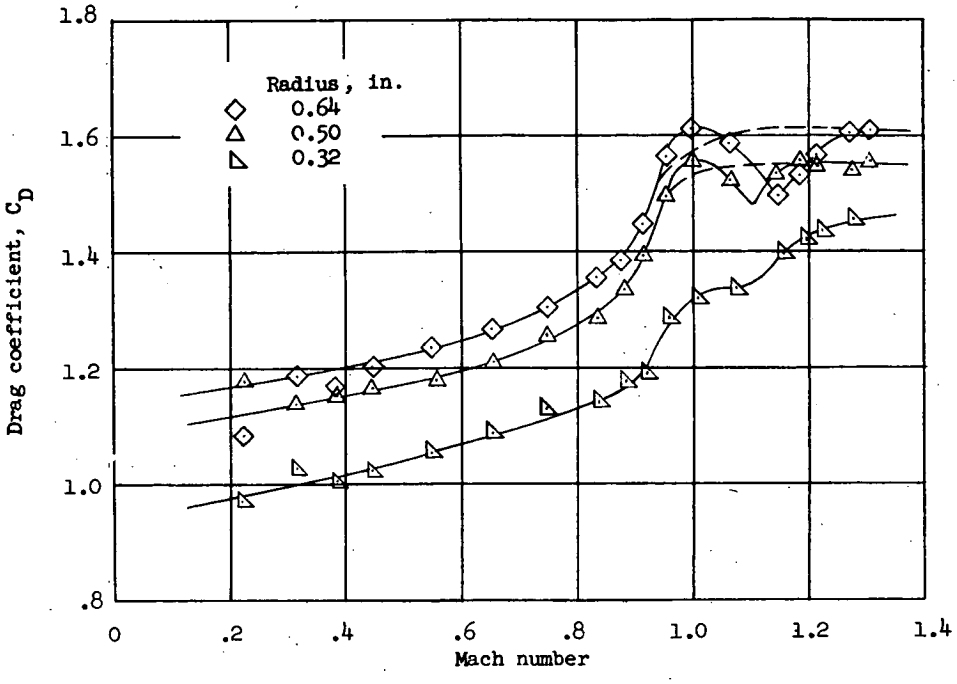


(a) Aspect ratio, 0.50.

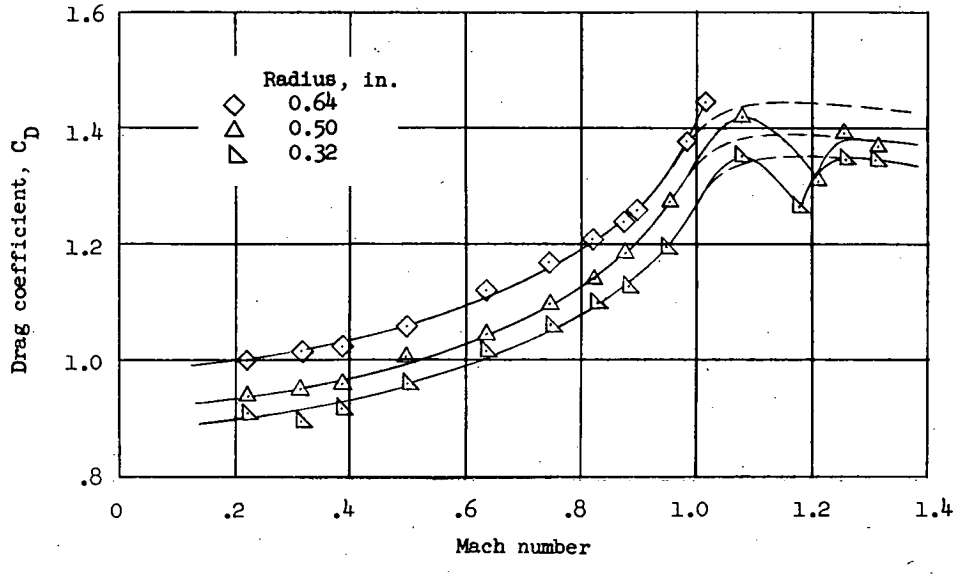


(b) Aspect ratio, 1.00.

Figure 7.- Variation of brake drag coefficient with Mach number for a deflection angle of 60°.

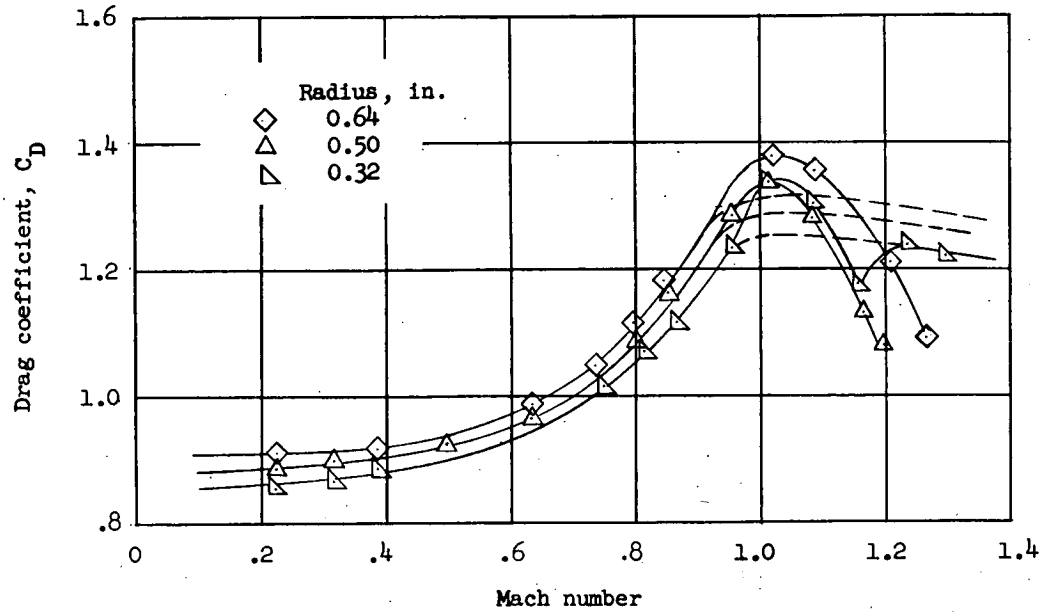


(c) Aspect ratio, 2.00.

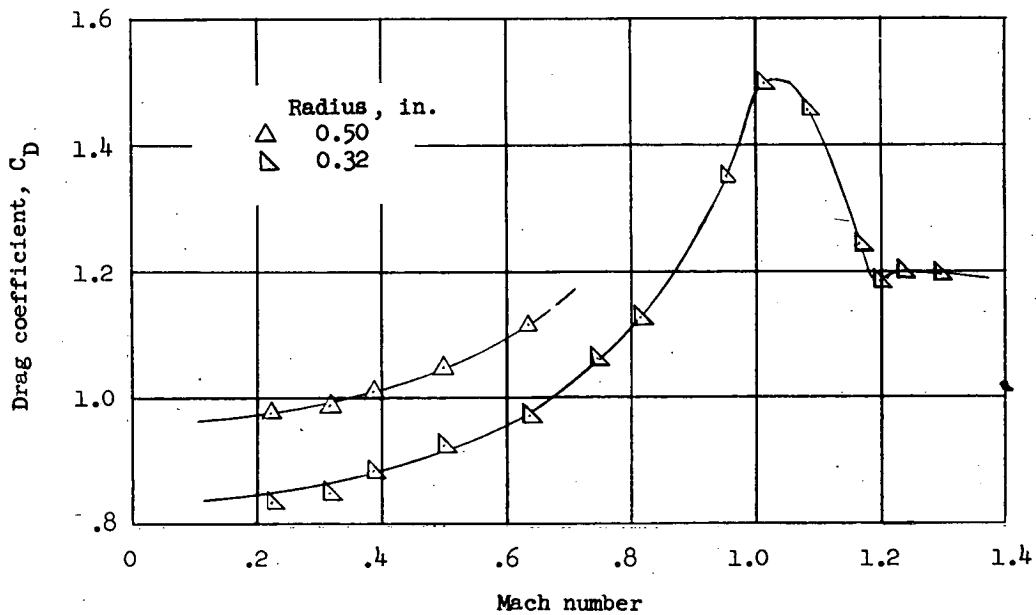


(d) Aspect ratio, 4.00.

Figure 7.- Concluded.

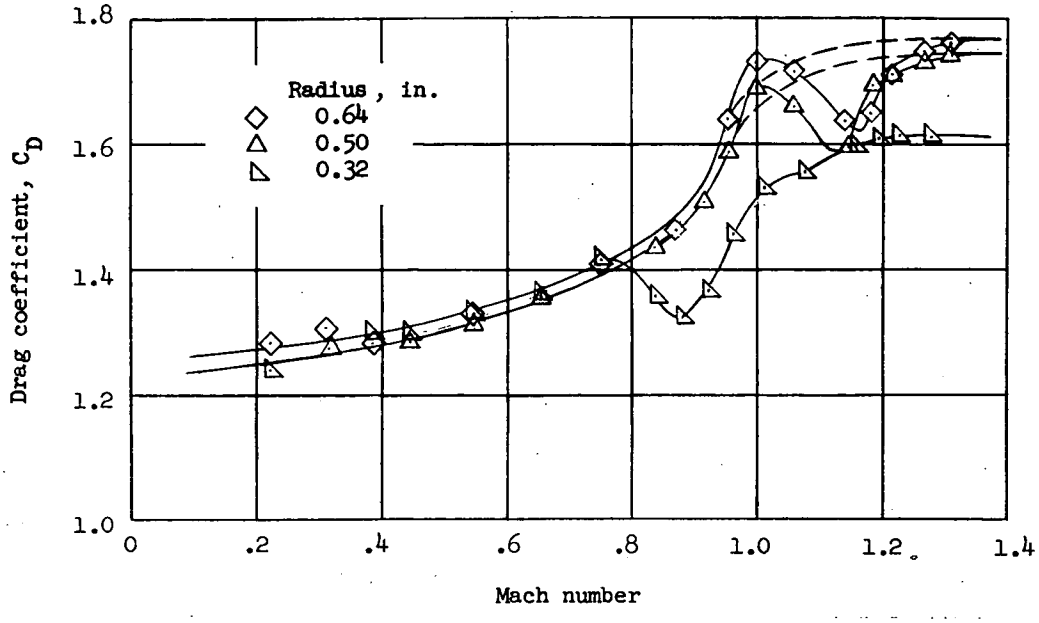


(a) Aspect ratio, 0.50.

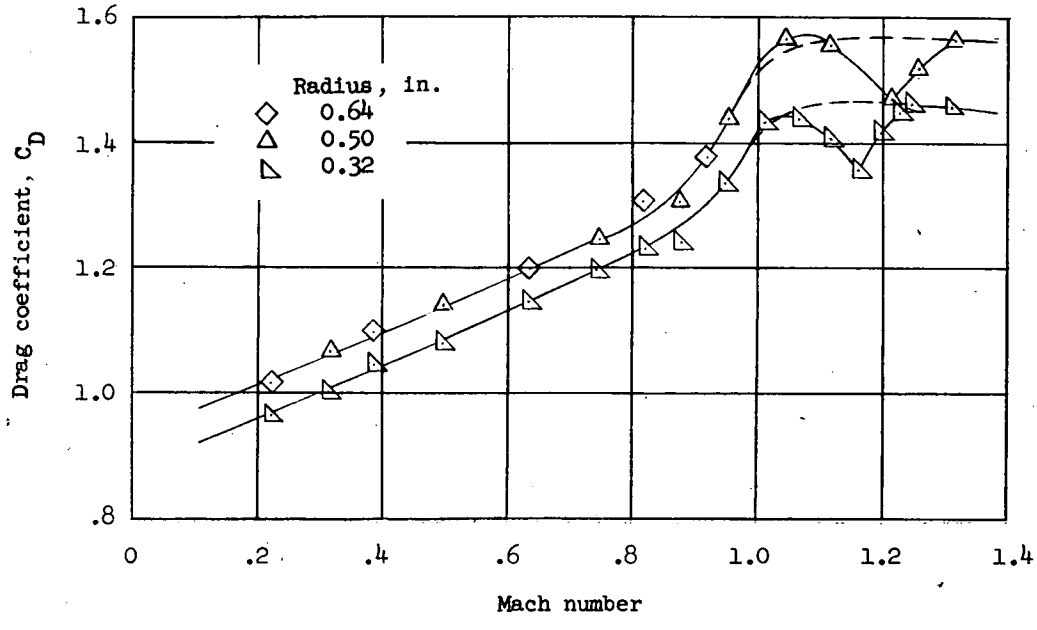


(b) Aspect ratio, 1.00.

Figure 8.- Variation of brake drag coefficient with Mach number for a deflection angle of 90°.

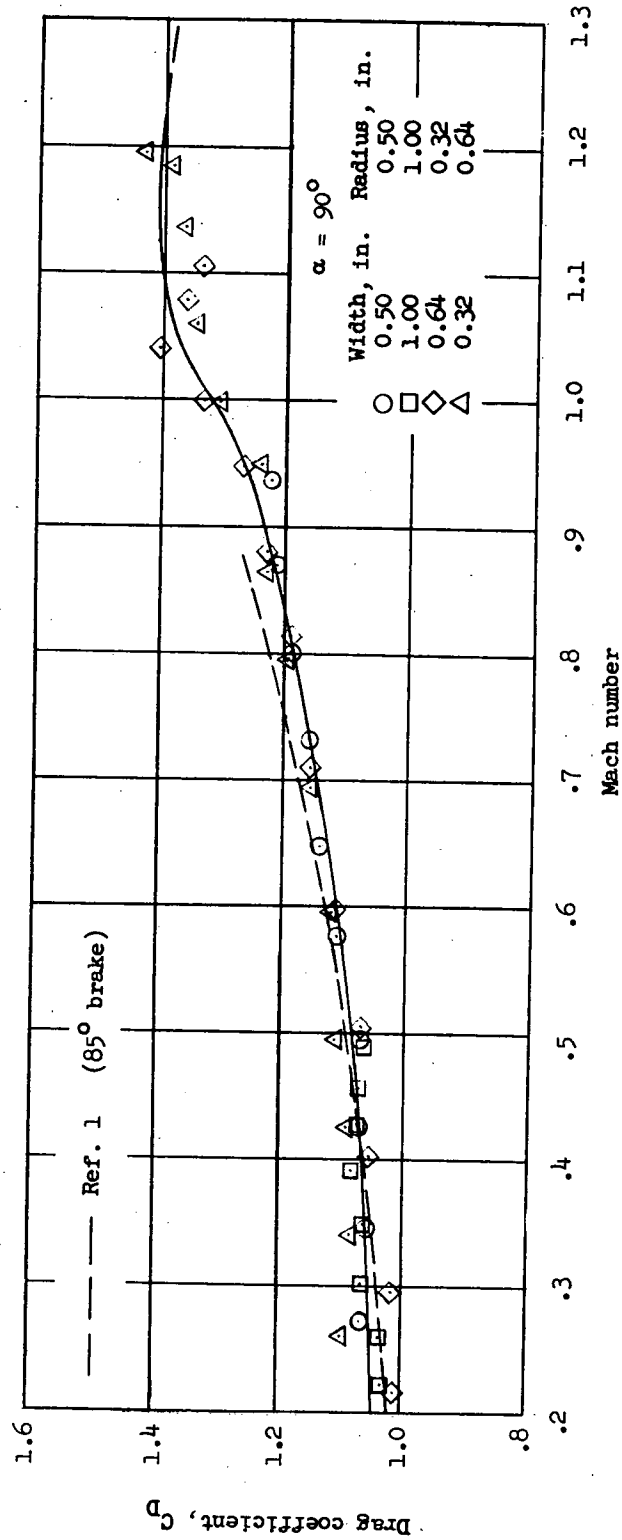


Figure 9.- Variation of sting-mounted flat-plate drag coefficient with Mach number.

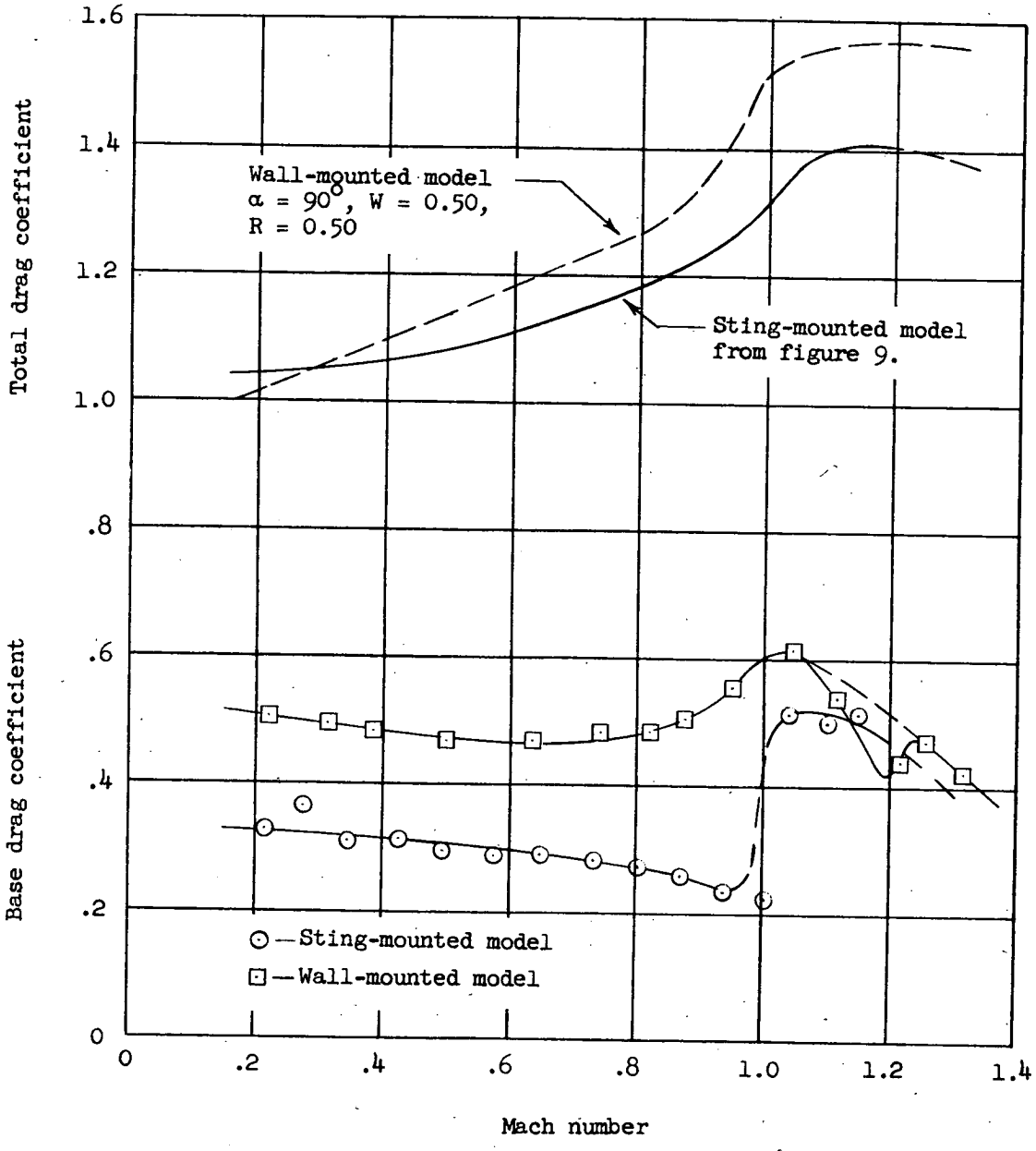


Figure 10.- Comparisons of total and base drag coefficients for two identical brakes, one sting mounted and the other wall mounted in the presence of a boundary layer.

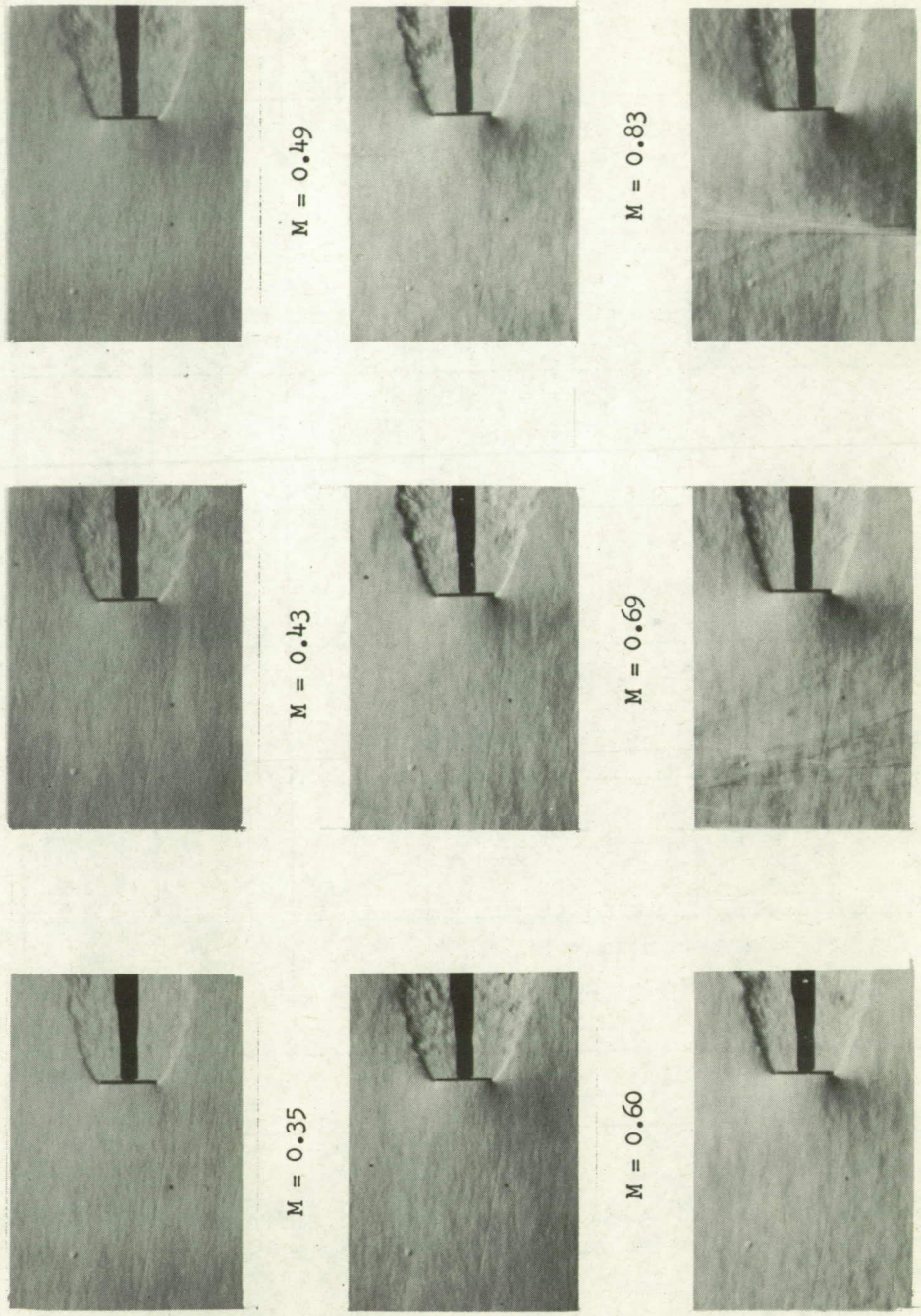


L-57-2777

(a) W = 1.00 inch; R = 1.00 inch.

Figure 11.- Schlieren photographs of sting-mounted flat plate with an aspect ratio of 1.00.

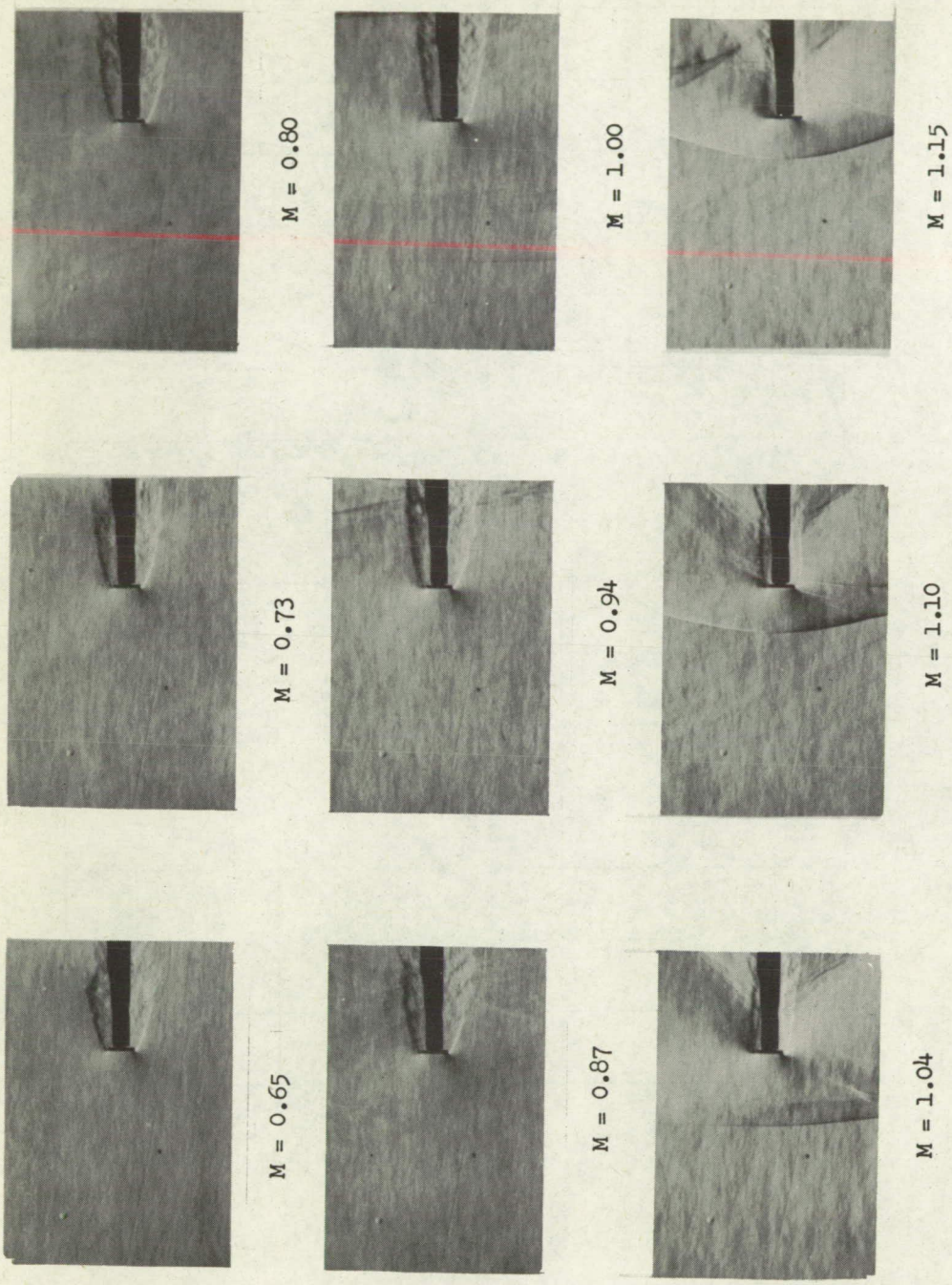


(b) W = 0.50 inch; R = 0.50 inch.

L-57-2778

Figure 11.- Concluded.

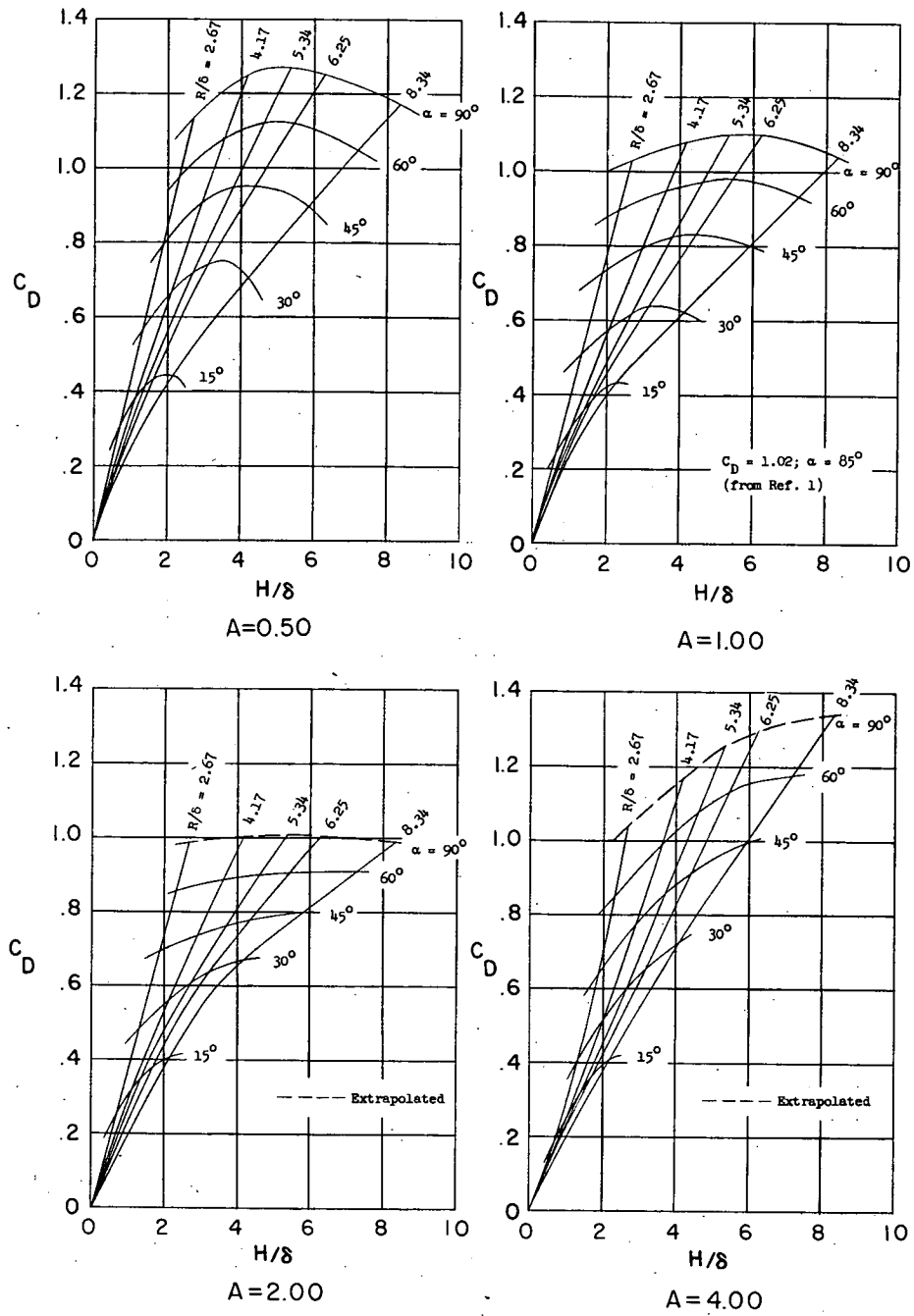


(a) M = 0.20.

Figure 12.- Design charts of $C_D$ plotted against $H/\delta$ for various aspect ratios.

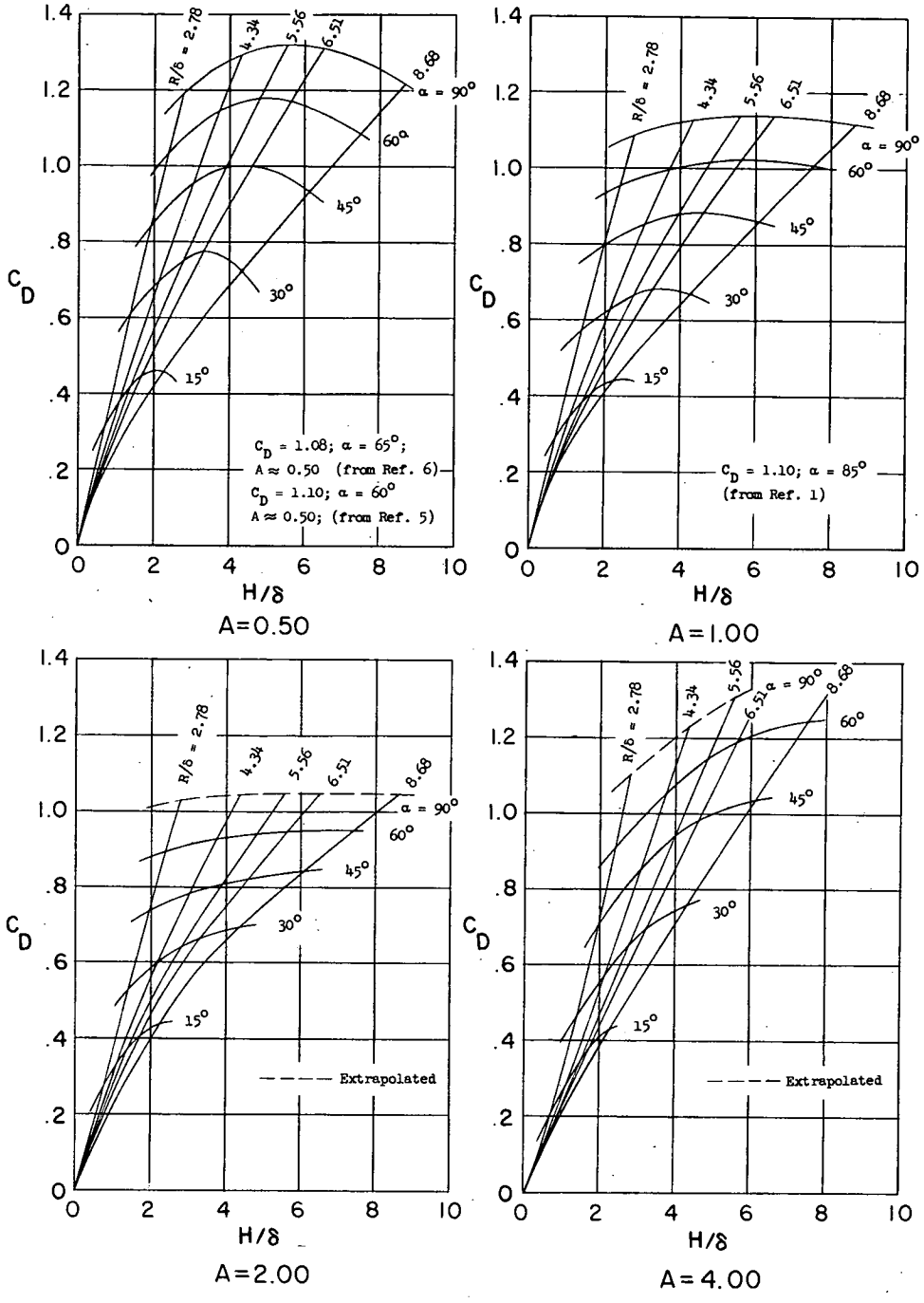


(b) M = 0.50.

Figure 12.- Continued.

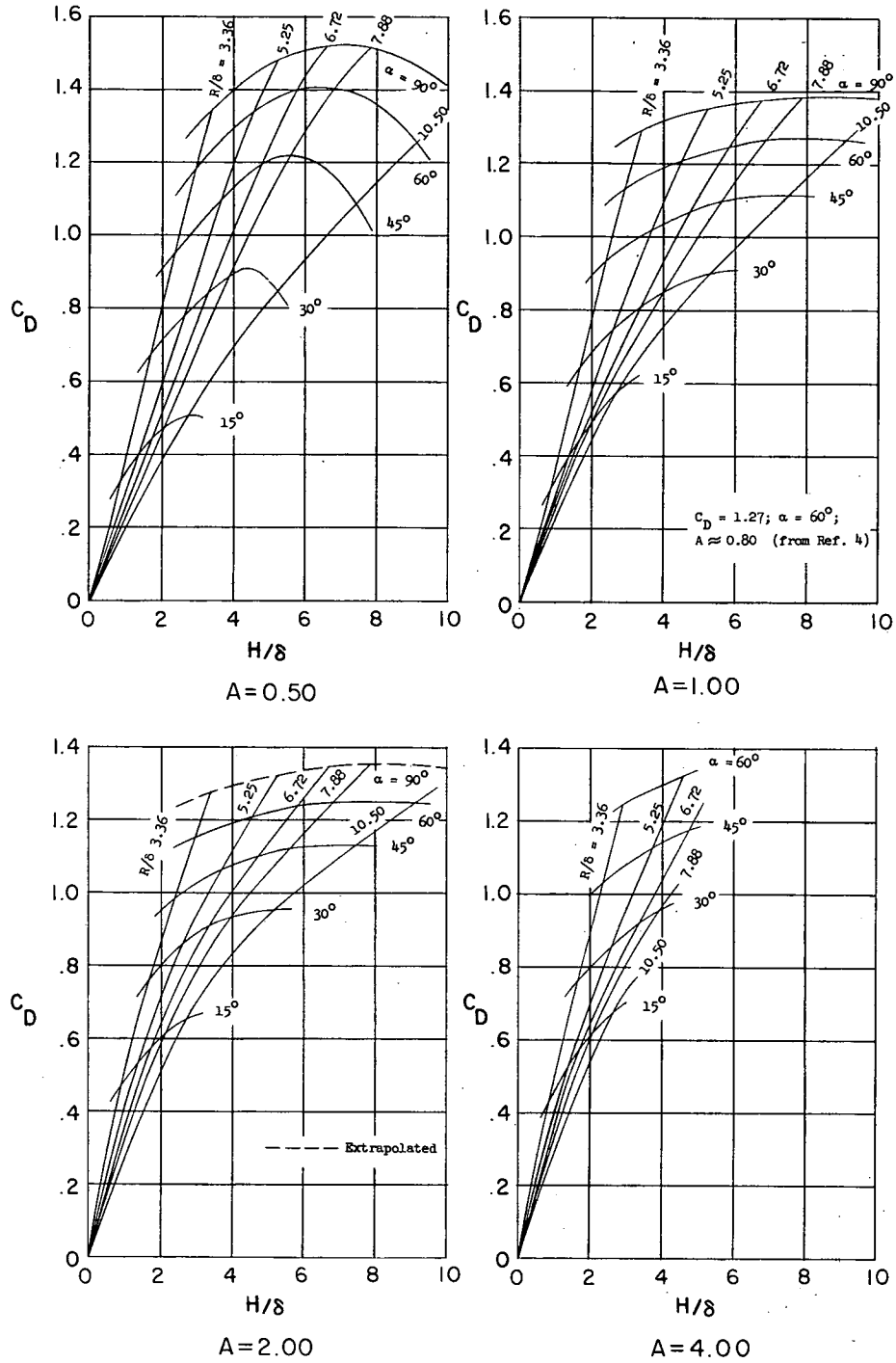


(c) M = 0.90.

Figure 12.- Continued.

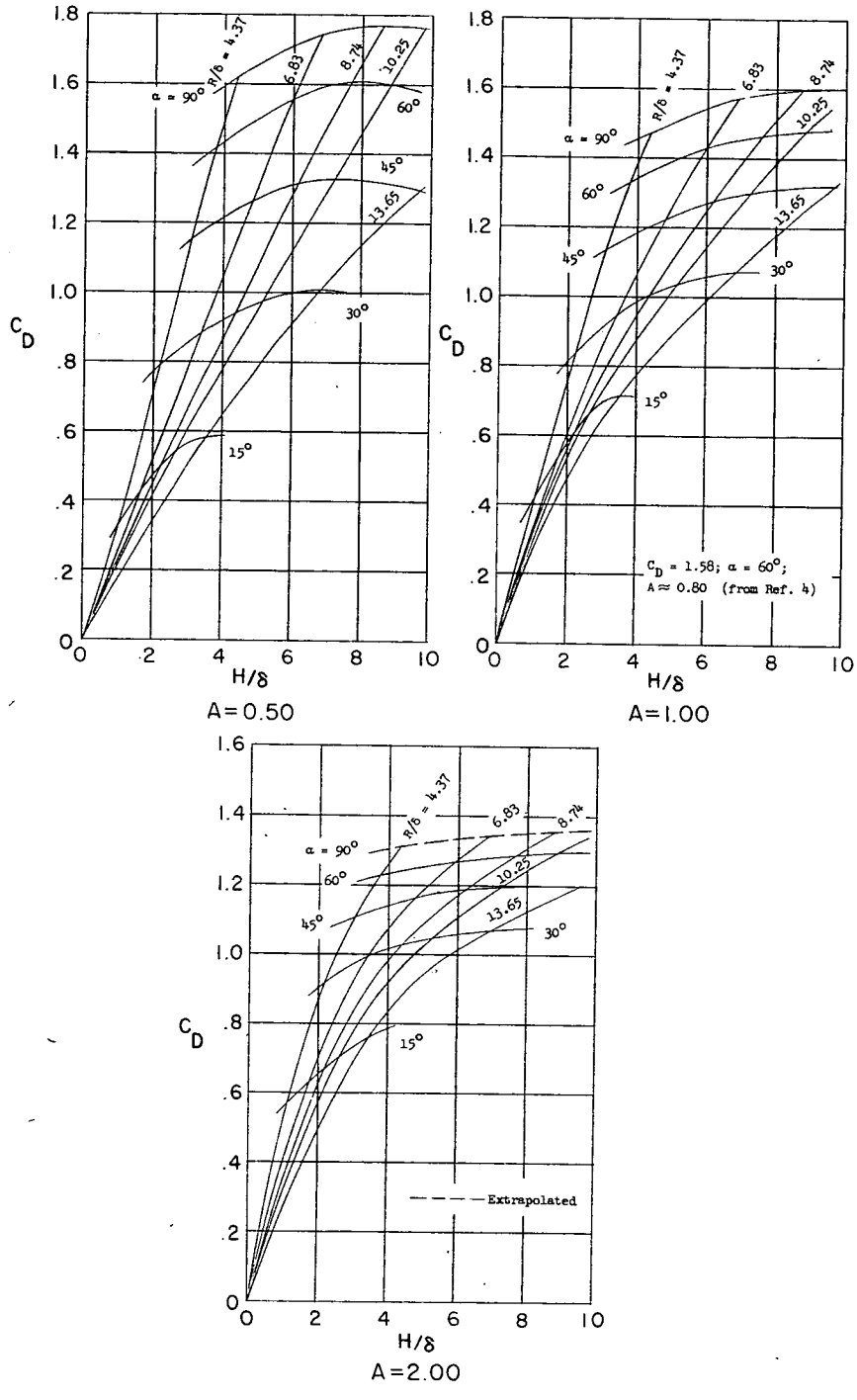


(d) M = 1.30.

Figure 12.- Concluded.

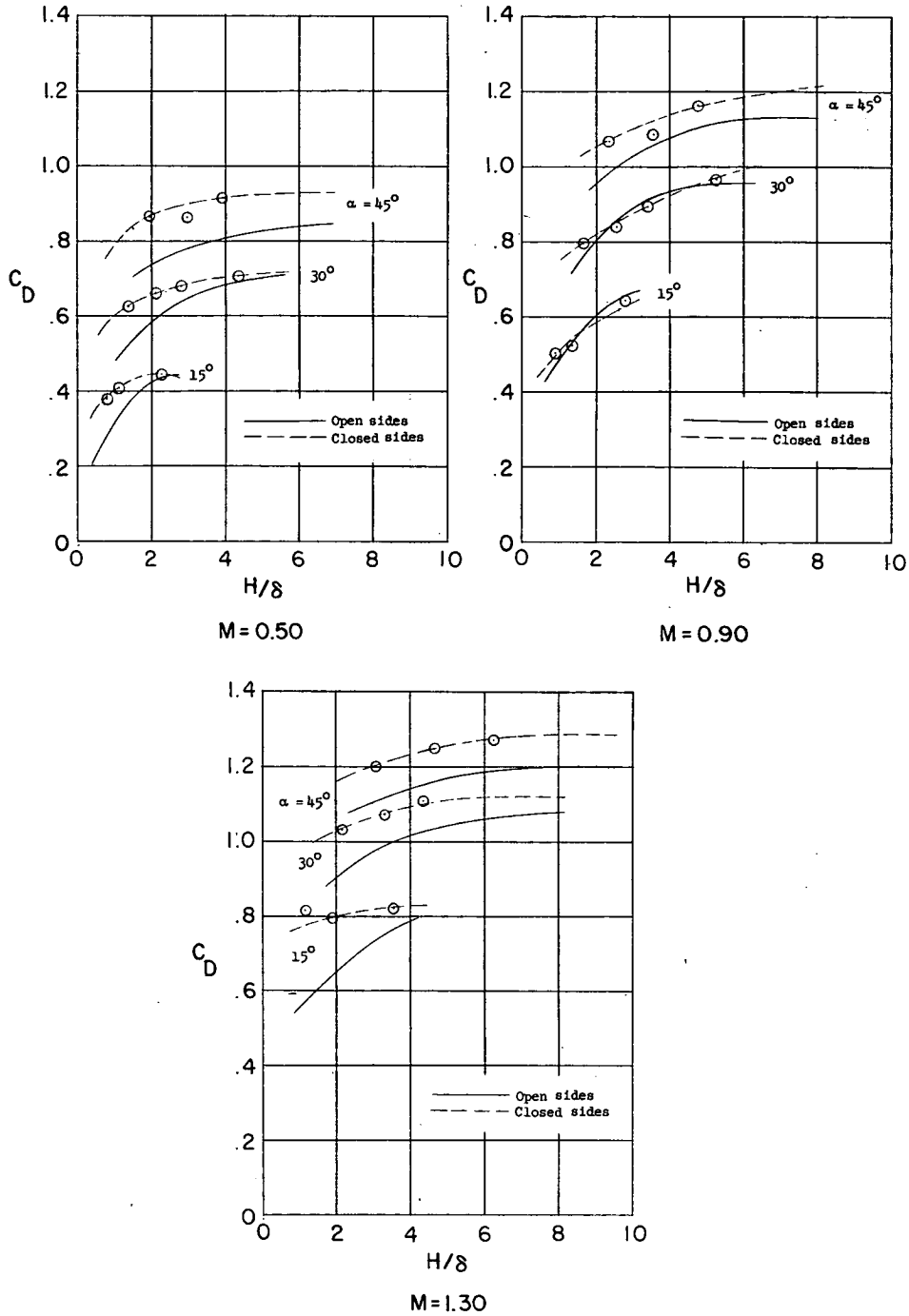


Figure 13.- Comparisons of $C_D$ plotted against $H/\delta$ for open- and closed-sided speed brakes at a constant aspect ratio of 2.00 for various Mach numbers.

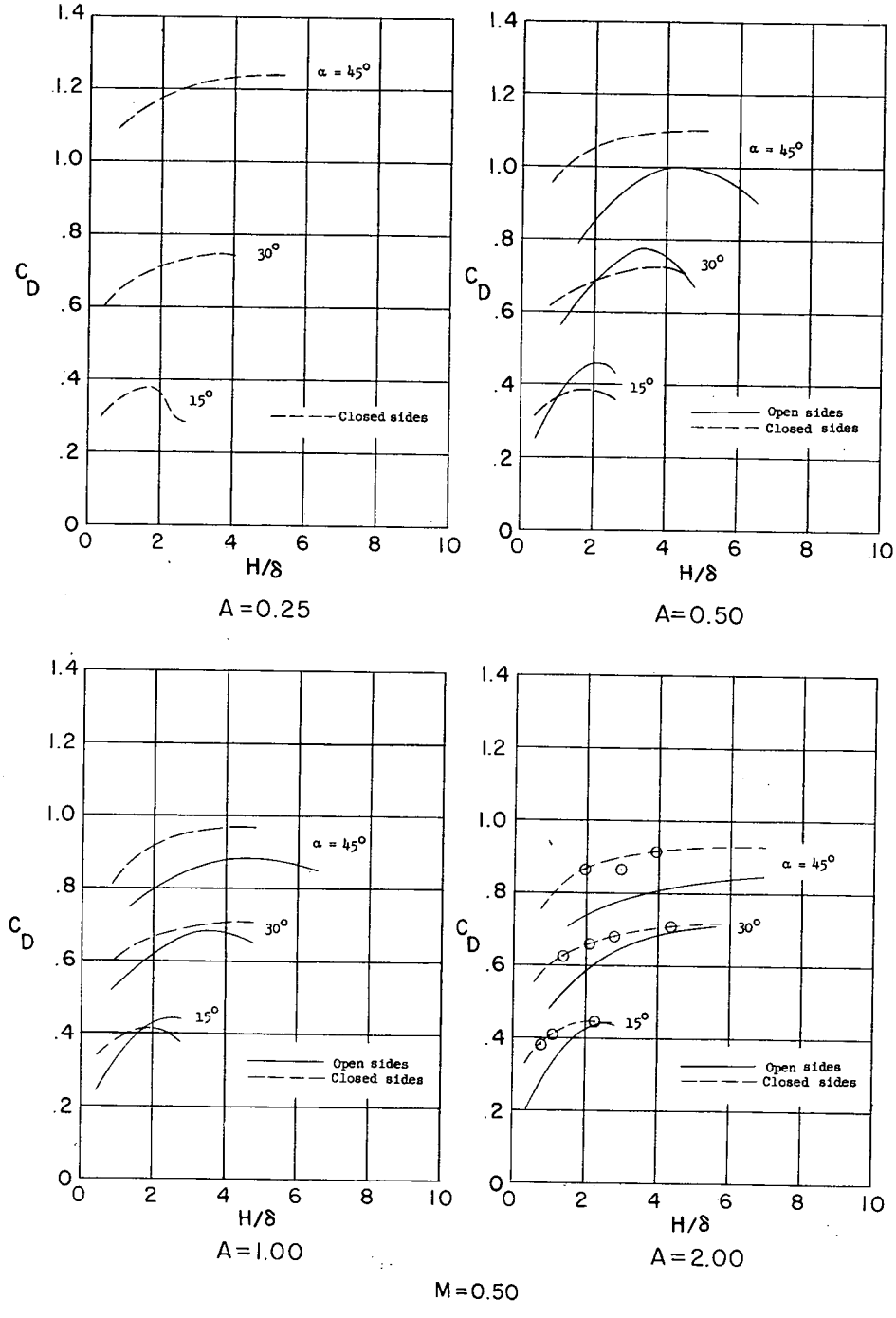


Figure 14.- Comparisons of $C_D$ plotted against $H/\delta$ for open- and closed-sided speed brakes at a constant Mach number of 0.50 for various aspect ratios.